Chapter 4
Geometry of Decoupled Serial Robots

4.1 Introduction

This chapter is devoted to the *displacement analysis* of robotic manipulators of the serial type, which we call the *geometry of serial robots*. The study is limited to *decoupled robots*, to be defined below, the inverse displacement analysis of general six-axis robots being the subject of Chap. 9. These robots serving mainly to perform *manipulation tasks*, they are also referred to as *manipulators*.

We begin by defining a serial, n-axis manipulator. In connection with this manipulator, additionally, we will (a) introduce the *Denavit–Hartenberg notation* for the definition of *link frames* that uniquely determine the *architecture* and the *configuration*, or *posture*, of the manipulator at hand; (b) define the *Cartesian* and *joint coordinates* of this manipulator; and (c) relate these two sets of variables by means of its *geometric model*. Moreover, with regard to six-axis manipulators, we will define *decoupled* manipulators and provide a procedure for the solution of their inverse displacement model.

4.2 The Denavit–Hartenberg Notation

One of the first tasks of a robotics engineer is the geometric modeling of a robotic manipulator. This task consists in devising a model that can be *unambiguously* (a) described to a control unit through a database and (b) interpreted by other robotics engineers. The purpose of this task is to give manipulating instructions to a robot, regardless of the dynamics of the manipulated load and the robot itself. The simplest way of geometrically modeling a robotic manipulator is by means of the concept of

Electronic supplementary material The online version of this article (doi: 10.1007/978-3-319-01851-5_4) contains supplementary material, which is available to authorized users.

J. Angeles, *Fundamentals of Robotic Mechanical Systems: Theory, Methods, and Algorithms*, Mechanical Engineering Series 124, DOI 10.1007/978-3-319-01851-5_4,

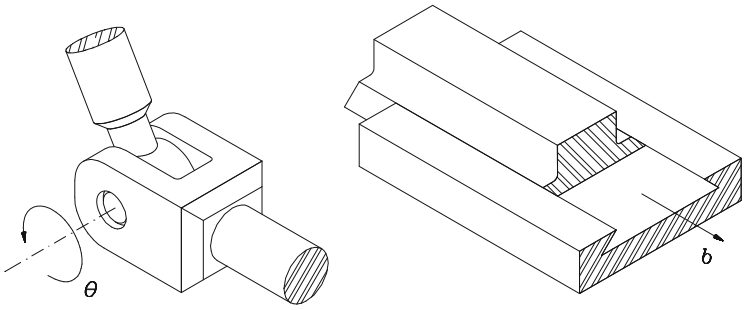

Fig. 4.1 The two basic lower kinematic pairs: the revolute and the prismatic joints

kinematic chain. A kinematic chain is a set of *rigid bodies*, also called *links*, coupled by *kinematic pairs*, also termed *joints*. A kinematic pair is, then, the coupling of two rigid bodies so as to constrain their relative motion. We distinguish two basic types of kinematic pairs, namely, *higher* and *lower* kinematic pairs. A higher kinematic pair arises between rigid bodies when contact takes place along a line or at a point. This type of coupling occurs in cam-and-follower mechanisms, gear trains, and roller bearings, for example. A lower kinematic pair occurs when contact takes place along a surface common to the two bodies. Six different types of lower kinematic pairs can be distinguished (Angeles 1982; Hartenberg and Denavit 1964), but all these can be produced from two basic types, namely, the *rotating pair*, denoted by *R* and also called *revolute*, and the *sliding pair*, represented by *P* and also called *prismatic*.

The common surface along which contact takes place in a revolute pair is commonly billed as a cylinder. However, a cylinder exhibits two kinds of symmetry, of revolution and of extrusion, a cylindrical surface thus allowing for both rotation about the axis of the cylinder and translation along a direction parallel to the axis. For this reason, an axially symmetric surface devoid of symmetry of extrusion was proposed by Khan and Angeles (2011). A typical realization of the revolute joint is the coupling through journal bearings. Thus, two rigid bodies coupled by a revolute can rotate relative to each other about the axis of the common cylinder, which is thus referred to as the *axis of the revolute*, but are prevented from undergoing relative translations as well as rotations about axes other than the cylinder axis. On the other hand, the common surface of contact between two rigid bodies coupled by a prismatic pair is a prism of arbitrary cross section, and hence, the two bodies coupled in this way are prevented from undergoing any relative rotation and can move only in a pure-translation motion along a direction parallel to the axis of the prism. As an example of this kinematic pair, one can cite the dovetail coupling. Note that whereas the revolute axis is a totally defined line in three-dimensional space, the *prismatic pair has no axis*; this pair has only a *direction*. That is, the prismatic pair does not have a particular location in space. Nevertheless, and for the sake of conciseness, we will refer to *joint axis* generically, when speaking of either revolute or prismatic joints. Bodies coupled by a revolute and a prismatic pair are shown in Fig. 4.1.

Serial manipulators will be considered in this chapter, their associated kinematic chains thus being of the *simple* type, i.e., each and every link is coupled to at most two other links. A *simple kinematic chain* can be either closed or open. It is closed if each and every link is coupled to two other links, the chain then being called a *linkage*; it is open if it contains exactly two links, the end ones, that are coupled to only one other link. Thus, simple kinematic chains studied in this chapter are open, and in the particular robotics terminology, their first link is called the *manipulator base*, whereas their last link is termed the *end-effector (EE)*.

Thus, the kinematic chains associated with manipulators of the serial type are composed of *binary links*, the intermediate ones, and exactly two *simple links*, those at the ends. Hence, except for the end links, all links carry two kinematic pairs, and as a consequence, two pair axes—just remember that a prismatic pair has a direction but no axis. In order to uniquely describe the *architecture* of a kinematic chain, i.e., the relative location and orientation of its neighboring pair axes, the Denavit–Hartenberg notation (Denavit and Hartenberg 1955) is introduced. To this end, links are numbered $0, 1, \ldots, n$, the ith pair being defined as that coupling the $(i-1)$st link with the ith link. Hence, the manipulator is assumed to be composed of $n+1$ links and n pairs; each of the latter can be either R or P, where link 0 is the fixed base, while link n is the end-effector. Next, a coordinate frame $\mathcal{F}_i$ is defined with origin O_i and axes X_i, Y_i, Z_i. This frame is attached to the $(i-1)$st link—**not** to the ith link!—for $i = 1, \ldots, n+1$. This is the classical Denavit–Hartenberg notation. Khalil and collaborators (Khalil and Dombre 2002) modified this notation to make it "less ambiguous." In the balance of the book we follow the classical notation. For the first n frames, this is done following the rules given below:

1. Z_i is the axis of the ith pair. Notice that there are two possibilities of defining the positive direction of this axis, since each pair axis is only a line, not a directed segment. Moreover, the Z_i axis of a prismatic pair can be located arbitrarily, since only its direction is defined.
2. X_i is defined as the common perpendicular to Z_{i-1} and Z_i, directed from the former to the latter, as shown in Fig. 4.2a. Notice that if these two axes intersect, the positive direction of X_i is undefined and hence, can be freely assigned. Henceforth, we will follow the *right-hand* rule in this case. This means that if unit vectors $\mathbf{i}_i$, $\mathbf{k}_{i-1}$, and $\mathbf{k}_i$ are attached to axes X_i, Z_{i-1}, and Z_i, respectively, as indicated in Fig. 4.2b, then $\mathbf{i}_i$ is defined as $\mathbf{k}_{i-1} \times \mathbf{k}_i$. Moreover, if Z_{i-1} and Z_i are parallel, the location of X_i is undefined. In order to define it uniquely, we will specify X_i as passing through the origin of the $(i-1)$st frame, as shown in Fig. 4.2c.
3. The *distance* between Z_i and Z_{i+1} is defined as a_i, which is thus *nonnegative*.
4. The Z_i-coordinate of the intersection O_i' of Z_i with X_{i+1} is denoted by b_i. Since this quantity is a coordinate, it can be either positive or negative. Its absolute value is the distance between X_i and X_{i+1}, also called the *offset* between successive common perpendiculars to the corresponding joint axes.
5. The angle between Z_i and Z_{i+1} is defined as α_i and is measured about the positive direction of X_{i+1}. This item is known as the *twist angle* between successive pair axes.

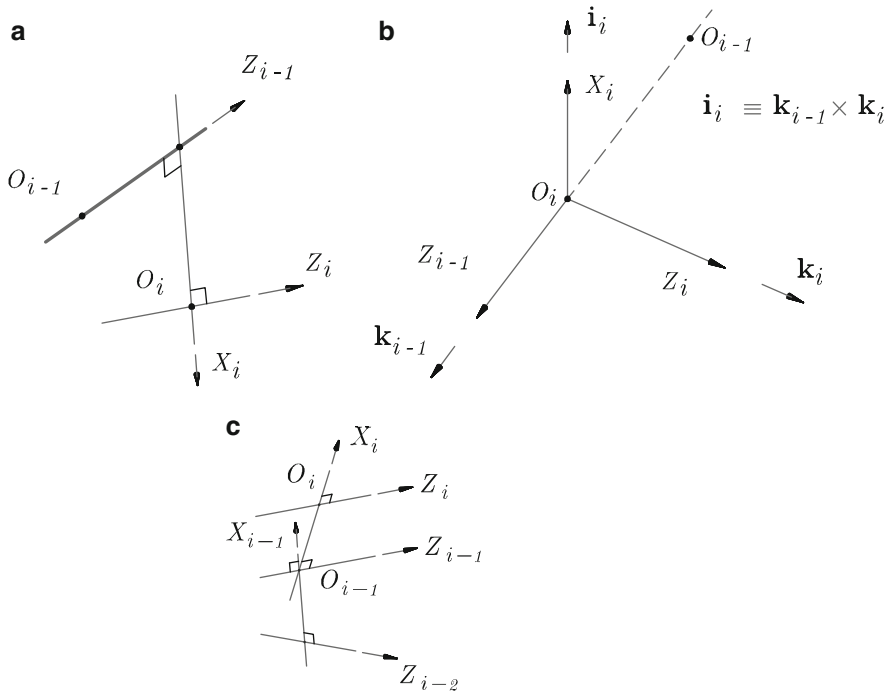

Fig. 4.2 Definition of X_i when Z_{i-1} and Z_i: (**a**) are skew; (**b**) intersect; and (**c**) are parallel

6. The angle between X_i and X_{i+1} is defined as θ_i and is measured about the positive direction of Z_i.

The $(n+1)$st coordinate frame is attached to the far end of the nth link. Since the manipulator has no $(n+1)$st link, the foregoing rules do not apply to the definition of this frame. The analyst, thus, has the freedom to define this frame as it best suits the task at hand. Notice that $n+1$ frames, $\mathcal{F}_1, \mathcal{F}_2, \ldots, \mathcal{F}_{n+1}$, have been defined, whereas links are numbered from 0 to n. In summary, a n-axis manipulator is composed of $n+1$ links and $n+1$ coordinate frames. These rules are illustrated with an example below.

Consider the architecture depicted in Fig. 4.3, usually referred to as a *Puma robot*, which shows seven links, numbered from 0 to 6, and seven coordinate frames, numbered from 1 to 7. Note that the last frame is arbitrarily defined, but its origin is placed at a specific point of the EE, namely, at the *operation point* P, which is used to define the task at hand. Furthermore, three axes intersect at a point C, and hence, all points of the last three links move on concentric spheres with respect to $\mathcal{F}_4$, for which reason the subchain comprising these three links is known as a *spherical wrist*, point C being its *center*. By the same token, the subchain composed of the first four links is called the *arm*. Thus, the wrist is *decoupled* from the arm, and is used for orientation purposes, the arm being used for the positioning of point C.

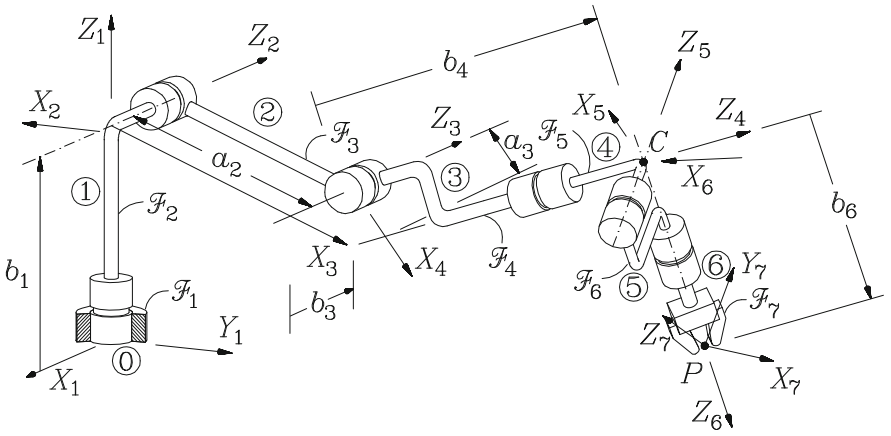

Fig. 4.3 Coordinate frames of a Puma robot

The arm is sometimes called the *regional structure* and the wrist the *local structure*, the overall manipulator thus being of the *decoupled* type.

In the foregoing discussion, if the ith pair is R, then all quantities involved in those definitions are constant, except for θ_i, which is variable and is thus termed the *joint variable* of the ith pair. The other quantities, i.e., a_i, b_i, and α_i, are the *joint parameters* of the same pair. If, alternatively, the ith pair is P, then b_i is variable, and the other quantities are constant. In this case, the joint variable is b_i, and the joint parameters are a_i, α_i, and θ_i. Notice that associated with each joint there are exactly one joint variable and three constant parameters. Hence, a n-axis manipulator has n joint variables—which are henceforth grouped in the n-dimensional vector $\boldsymbol{\theta}$, regardless of whether the joint variables are angular or translational—and $3n$ constant parameters. The latter define the *architecture* of the manipulator, while the former determine its *configuration*, or *posture*.

Whereas the manipulator architecture is fully defined by its $3n$ *Denavit–Hartenberg (DH) parameters*, its posture is fully defined by its n joint variables, also called its *joint coordinates*, once the DH parameters are known. The relative pose—position and orientation—between links is fully specified, then, from the background of Chap. 2, by (a) the rotation matrix taking the X_i, Y_i, Z_i axes into a configuration in which they are parallel pairwise to the X_{i+1}, Y_{i+1}, Z_{i+1} axes, and (b) the position vector of the origin of the latter in the former. The representations of the foregoing items in coordinate frame $\mathcal{F}_i$ will be discussed presently. First, we obtain the matrix representation of the rotation $\mathbf{Q}_i$ carrying $\mathcal{F}_i$ into an orientation coincident with that of $\mathcal{F}_{i+1}$, assuming, without loss of generality because we are interested only in changes of orientation, that the two origins are coincident, as depicted in Fig. 4.4. This matrix is most easily derived if the rotation of interest is decomposed into two successive rotations, as indicated in Fig. 4.5. In that figure, X_i', Y_i', Z_i' is an intermediate coordinate frame $\mathcal{F}_i'$, obtained by rotating $\mathcal{F}_i$ about

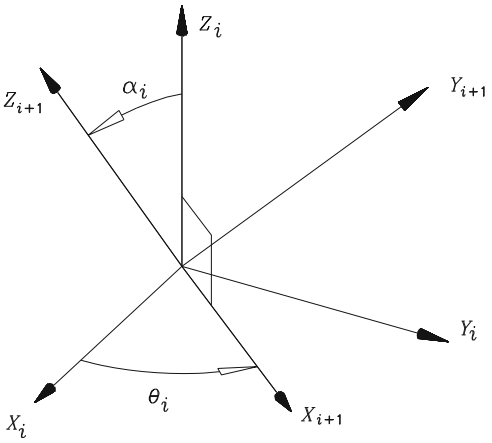

Fig. 4.4 Relative orientation of the ith and $(i+1)$st coordinate frames

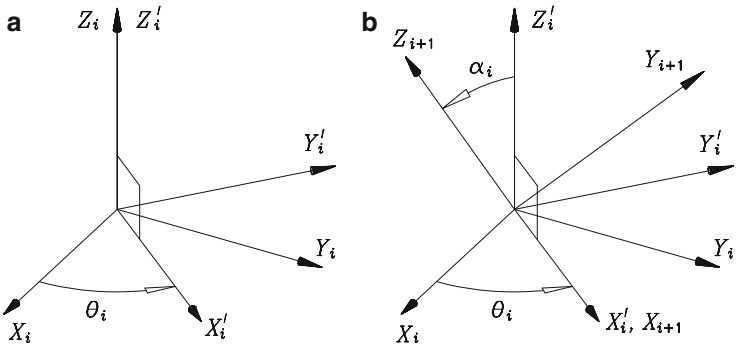

Fig. 4.5 (**a**) Rotation about axis Z_i through an angle θ_i; and (**b**) relative orientation of the i'th and the $(i+1)$st coordinate frames

the Z_i axis through an angle θ_i. Then, the intermediate frame is rotated about $X_{i'}$ through an angle α_i, which takes it into a configuration coincident with $\mathcal{F}_{i+1}$. Let the foregoing rotations be denoted by $[\,\mathbf{C}_i\,]_i$ and $[\,\mathbf{\Lambda}_i\,]_{i'}$, respectively, which are readily derived for they are in the canonical forms (2.56c) and (2.56a), respectively.

Moreover, let

$$\lambda_i \equiv \cos\alpha_i, \quad \mu_i \equiv \sin\alpha_i \tag{4.1a}$$

One thus has, using subscripted brackets as introduced in Sect. 2.2,

$$[\,\mathbf{C}_i\,]_i = \begin{bmatrix} \cos\theta_i & -\sin\theta_i & 0 \\ \sin\theta_i & \cos\theta_i & 0 \\ 0 & 0 & 1 \end{bmatrix}, \quad [\,\mathbf{\Lambda}_i\,]_{i'} = \begin{bmatrix} 1 & 0 & 0 \\ 0 & \lambda_i & -\mu_i \\ 0 & \mu_i & \lambda_i \end{bmatrix} \tag{4.1b}$$

and hence, the matrix sought is computed simply as

$$[\,\mathbf{Q}_i\,]_i = [\,\mathbf{C}_i\,]_i\,[\,\mathbf{\Lambda}_i\,]_{i'} \tag{4.1c}$$

Henceforth, we will use the abbreviations introduced below:

$$\mathbf{Q}_i \equiv [\,\mathbf{Q}_i\,]_i, \quad \mathbf{C}_i \equiv [\,\mathbf{C}_i\,]_i, \quad \mathbf{\Lambda}_i \equiv [\,\mathbf{\Lambda}_i\,]_{i'} \tag{4.1d}$$

thereby doing away with brackets, when these are self-understood. Thus,

$$\mathbf{Q}_i \equiv [\,\mathbf{Q}_i\,]_i \equiv \begin{bmatrix} \cos\theta_i & -\lambda_i \sin\theta_i & \mu_i \sin\theta_i \\ \sin\theta_i & \lambda_i \cos\theta_i & -\mu_i \cos\theta_i \\ 0 & \mu_i & \lambda_i \end{bmatrix} \tag{4.1e}$$

One more factoring of matrix $\mathbf{Q}_i$, which will be used in Chap. 9, is given below:

$$\mathbf{Q}_i = \mathbf{Z}_i \mathbf{X}_i \tag{4.2a}$$

with $\mathbf{X}_i$ and $\mathbf{Z}_i$ defined as two *pure reflections*, the former about the $Y_i Z_i$ plane, the latter about the $X_i Y_i$ plane, namely,

$$\mathbf{X}_i \equiv \begin{bmatrix} 1 & 0 & 0 \\ 0 & -\lambda_i & \mu_i \\ 0 & \mu_i & \lambda_i \end{bmatrix}, \quad \mathbf{Z}_i \equiv \begin{bmatrix} \cos\theta_i & \sin\theta_i & 0 \\ \sin\theta_i & -\cos\theta_i & 0 \\ 0 & 0 & 1 \end{bmatrix} \tag{4.2b}$$

Note that both $\mathbf{X}_i$ and $\mathbf{Z}_i$ are symmetric and self-inverse—see Sect. 2.2. In order to derive an expression for the position vector $\mathbf{a}_i$ connecting the origin O_i of $\mathcal{F}_i$ with that of $\mathcal{F}_{i+1}$, O_{i+1}, reference is made to Fig. 4.6, showing the relative positions of the different origins and axes involved. From this figure, apparently,

$$\mathbf{a}_i \equiv \overrightarrow{O_i O_{i+1}} = \overrightarrow{O_i O_i'} + \overrightarrow{O_i' O_{i+1}} \tag{4.3a}$$

where obviously,

$$[\,\overrightarrow{O_i O_i'}\,]_i = \begin{bmatrix} 0 \\ 0 \\ b_i \end{bmatrix}, \quad [\,\overrightarrow{O_i' O_{i+1}}\,]_{i+1} = \begin{bmatrix} a_i \\ 0 \\ 0 \end{bmatrix}$$

Now, in order to compute the sum appearing in Eq. (4.3a), the two foregoing vectors should be expressed in the same coordinate frame, namely, $\mathcal{F}_i$. Thus,

$$[\,\overrightarrow{O_i' O_{i+1}}\,]_i = [\,\mathbf{Q}_i\,]_i\,[\,\overrightarrow{O_i' O_{i+1}}\,]_{i+1} = \begin{bmatrix} a_i \cos\theta_i \\ a_i \sin\theta_i \\ 0 \end{bmatrix}$$

and hence,

$$[\,\mathbf{a}_i\,]_i = \begin{bmatrix} a_i \cos\theta_i \\ a_i \sin\theta_i \\ b_i \end{bmatrix} \tag{4.3b}$$

For brevity, we introduce one more definition:

$$\mathbf{a}_i \equiv [\,\mathbf{a}_i\,]_i \tag{4.3c}$$

Similar to the foregoing factoring of $\mathbf{Q}_i$, vector $\mathbf{a}_i$ admits the factoring

$$\mathbf{a}_i = \mathbf{Q}_i \mathbf{b}_i \tag{4.3d}$$

where $\mathbf{b}_i$ is given by

$$\mathbf{b}_i \equiv \begin{bmatrix} a_i \\ b_i \mu_i \\ b_i \lambda_i \end{bmatrix} \tag{4.3e}$$

with the definitions introduced in Eq. (4.1a). Hence, vector $\mathbf{b}_i$ is constant for revolute pairs. From the geometry of Fig. 4.6, it should be apparent that $\mathbf{b}_i$ is nothing but $\mathbf{a}_i$ in $\mathcal{F}_{i+1}$, i.e.,

$$\mathbf{b}_i = [\mathbf{a}_i]_{i+1}\,.$$

Matrices $\mathbf{Q}_i$ can also be regarded as coordinate transformations. Indeed, let $\mathbf{i}_i$, $\mathbf{j}_i$, and $\mathbf{k}_i$ be the unit vectors parallel to the X_i, Y_i, and Z_i axes, respectively, directed in the positive direction of these axes. From Fig. 4.6, it is apparent that

$$[\,\mathbf{i}_{i+1}\,]_i = \begin{bmatrix} \cos\theta_i \\ \sin\theta_i \\ 0 \end{bmatrix}, \quad [\,\mathbf{k}_{i+1}\,]_i = \begin{bmatrix} \mu_i \sin\theta_i \\ -\mu_i \cos\theta_i \\ \lambda_i \end{bmatrix}$$

whence

$$[\,\mathbf{j}_{i+1}\,]_i = [\,\mathbf{k}_{i+1} \times \mathbf{i}_{i+1}\,]_i = \begin{bmatrix} -\lambda_i \sin\theta_i \\ \lambda_i \cos\theta_i \\ \mu_i \end{bmatrix}$$

Therefore, the components of $\mathbf{i}_{i+1}$, $\mathbf{j}_{i+1}$, and $\mathbf{k}_{i+1}$ in $\mathcal{F}_i$ are nothing but the first, second, and third columns of $\mathbf{Q}_i$. In general, then, any vector $\mathbf{v}$ in $\mathcal{F}_{i+1}$ is transformed into $\mathcal{F}_i$ in the form

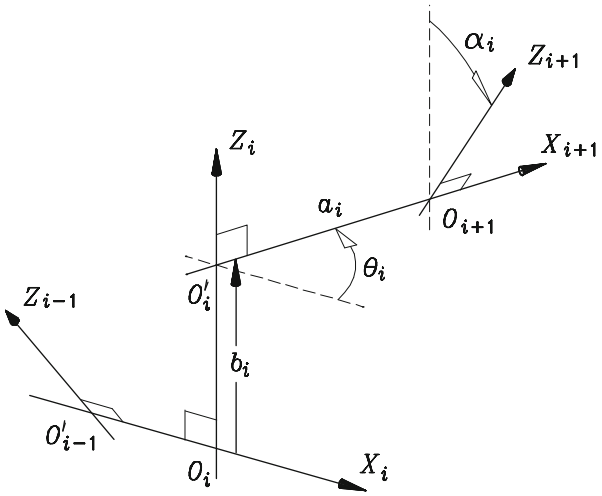

Fig. 4.6 Layout of three successive coordinate frames

$$[\mathbf{v}]_i = [\mathbf{Q}_i]_i [\mathbf{v}]_{i+1}$$

which is a similarity transformation, as defined in Eq. (2.118). Likewise, any matrix $\mathbf{M}$ in $\mathcal{F}_{i+1}$ is transformed into $\mathcal{F}_i$ by the corresponding similarity transformation, as given by Eq. (2.128):

$$[\mathbf{M}]_i = [\mathbf{Q}_i]_i [\mathbf{M}]_{i+1} [\mathbf{Q}_i^T]_i$$

The inverse relations follow immediately in the form

$$[\mathbf{v}]_{i+1} = [\mathbf{Q}_i^T]_i [\mathbf{v}]_i, \quad [\mathbf{M}]_{i+1} = [\mathbf{Q}_i^T]_i [\mathbf{M}]_i [\mathbf{Q}_i]_i$$

or, upon recalling the first of definitions (4.1d),

$$[\mathbf{v}]_i = \mathbf{Q}_i [\mathbf{v}]_{i+1}, \quad [\mathbf{M}]_i = \mathbf{Q}_i [\mathbf{M}]_{i+1} \mathbf{Q}_i^T \tag{4.4a}$$

$$[\mathbf{v}]_{i+1} = \mathbf{Q}_i^T [\mathbf{v}]_i, \quad [\mathbf{M}]_{i+1} = \mathbf{Q}_i^T [\mathbf{M}]_i \mathbf{Q}_i \tag{4.4b}$$

Moreover, if we have a chain of i frames, $\mathcal{F}_1, \mathcal{F}_2, \ldots, \mathcal{F}_i$, then the *inward* coordinate transformation from $\mathcal{F}_i$ to $\mathcal{F}_1$ is given by

$$[\mathbf{v}]_1 = \mathbf{Q}_1 \mathbf{Q}_2 \cdots \mathbf{Q}_{i-1} [\mathbf{v}]_i \tag{4.5a}$$

$$[\mathbf{M}]_1 = \mathbf{Q}_1 \mathbf{Q}_2 \cdots \mathbf{Q}_{i-1} [\mathbf{M}]_i (\mathbf{Q}_1 \mathbf{Q}_2 \cdots \mathbf{Q}_{i-1})^T \tag{4.5b}$$

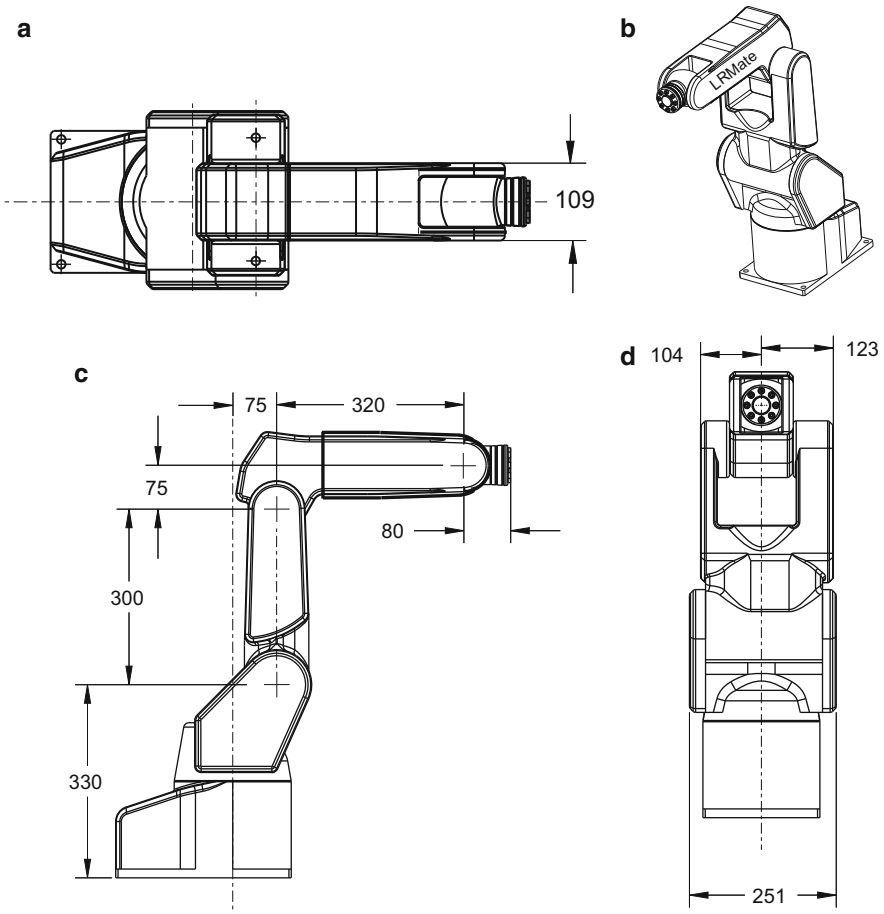

Fig. 4.7 The data sheet of the FANUC LRMate 200*i*C robot, with all dimensions in mm: (**a**) top view; (**b**) orthographic projection; (**c**) side view; and (**d**) front view

Likewise, the outward coordinate transformation takes the form

$$[\mathbf{v}]_i = (\mathbf{Q}_1\mathbf{Q}_2\cdots\mathbf{Q}_{i-1})^T[\mathbf{v}]_1 \tag{4.6a}$$

$$[\mathbf{M}]_i = (\mathbf{Q}_1\mathbf{Q}_2\cdots\mathbf{Q}_{i-1})^T[\mathbf{M}]_1\mathbf{Q}_1\mathbf{Q}_2\cdots\mathbf{Q}_{i-1} \tag{4.6b}$$

Example 4.2.1. The data sheet of the six-axis FANUC LR Mate 200*i*C robot is displayed in Fig. 4.7. Define seven coordinate frames, according with the Denavit–Hartenberg notation, with $\mathcal{F}_1$ fixed to the base and $\mathcal{F}_7$ to the EE. Then, produce a table containing the 18 (constant) Denavit–Hartenberg parameters of the robot.

Solution: First, the seven Z_i-axes are identified. Going from the base upwards, Z_1 is vertical, while Z_2 and Z_3 are horizontal, 300 mm apart, as per the side view, Z_1

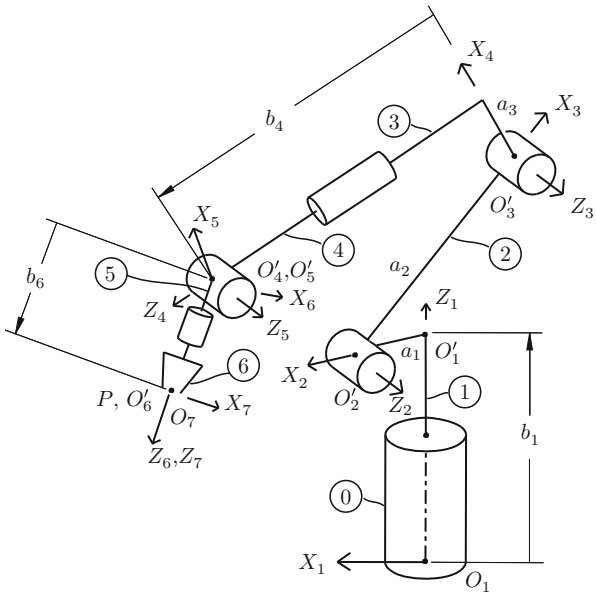

Fig. 4.8 The kinematic chain of the FANUC LRMate 200*i*C robot at an arbitrary posture

lying 75 mm from the vertical plane defined by Z_2 and Z_3. Z_4 appears horizontal in Fig. 4.7, 75 mm above Z_3, but it can attain other orientations. Moreover, Z_5 is also displayed horizontal in Fig. 4.7 parallel to Z_2 and Z_3; however, since Z_4 turns the link to which Z_5 is fixed, the one with the robot name painted in the orthographic projection, Z_5, in general, is not parallel to the two forgoing axes, Furthermore, in the same figure, Z_6, the axis of symmetry of the end plate, to which the EE is rigidly attached, is shown coincident with Z_4, but in general, these two axes intersect, together with Z_5, at the point located in the side view 80 mm from the plane of the end plate and $(330 + 300 + 75 =)705$ mm from the plane of the base. The point at which Z_4, Z_5 and Z_6 intersect is the center C of the wrist. To ease the definition of the DH parameters, the robot kinematic chain is displayed in Fig. 4.8 in an arbitrary posture. With the Z_i axes, for $i = 1, \ldots, 6$, identified, Z_7 is defined as coinciding with Z_6 for simplicity, as this axis is not bound by the DH notation. Likewise, X_1 can be defined arbitrarily, as long as it (a) is horizontal and (b) intersects Z_1. Finally, X_7 can also be defined arbitrarily, as long as it intersects Z_7 at right angles. In the next step, the X_i-axes are defined according with the DH notation. Once all 14 axes are defined, the definition of the DH parameters is straightforward: the a_i parameters are simple, b_i are less so, but their determination is eased once the O'_i intersections have been identified. These parameters are listed in Table 4.1.

Table 4.1 The DH parameters of the FANUC LRMate 200*i*C robot

i	a_i (mm)	b_i (mm)	$\alpha_i\,(^\circ)$
1	75	330	−90
2	300	0	0
3	75	0	−90
4	0	320	90
5	0	0	90
6	0	80	0

4.3 The Geometric Model of Six-Revolute Manipulators

The kinematics of serial manipulators begins with the study of the geometric relations between *joint variables* and *Cartesian variables*. The former were defined in Sect. 4.2 as those determining the posture of a given manipulator, with one such variable per joint; a six-axis manipulator, like the one displayed in Fig. 4.9, thus has six joint variables, $\theta_1, \theta_2, \ldots, \theta_6$. The Cartesian variables of a manipulator, in turn, are those variables defining the pose of the EE; since six independent variables are needed to define the pose of a rigid body, the manipulator of Fig. 4.9 thus involves six Cartesian variables.

The study outlined above pertains to the *geometry* of the manipulator, for it involves one single pose of the EE. Besides geometry, the kinematics of manipulators comprises the study of the relations between the time-rates of change of the joint variables, referred to as the *joint rates*, and the twist of the EE. Additionally, the relations between the second time-derivatives of the joint variables, referred to as the *joint accelerations*, with the time-rate of change of the twist of the EE also pertain to robot kinematics.

In the balance of this chapter we study the geometry of manipulators, the relations between joint rates, joint accelerations and their Cartesian counterparts, twist and twist-rate, being the subject of Chap. 5. In this regard, we distinguish two problems, commonly referred to as the *direct* and the *inverse* displacement

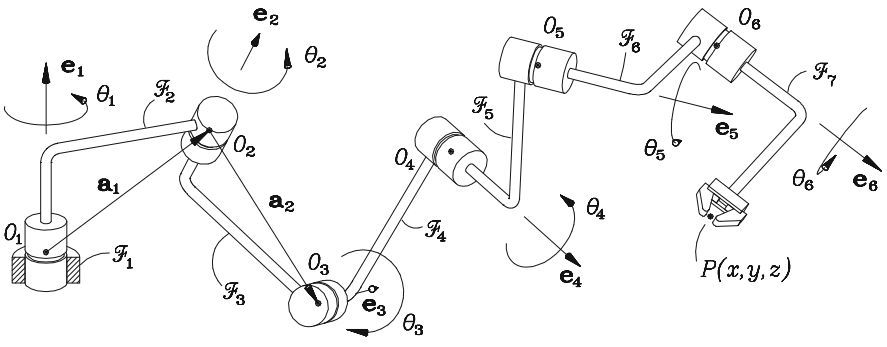

Fig. 4.9 Serial six-axis manipulator

problems, or DDP and correspondingly, IDP, for brevity. In the DDP, the six joint variables of a given six-axis manipulator are assumed to be known, the problem consisting in finding the pose of the EE. In the IDP, on the contrary, the pose of the EE is given, while the six joint variables that produce this pose are to be found.

The DDP reduces to matrix and matrix-times-vector multiplications; as we shall show presently, the DDP poses no major problem. The IDP, however, is more challenging, for it involves intensive variable-elimination and nonlinear-equation solving. Indeed, in the most general case, the IDP amounts to eliminating five out of the six unknowns, with the aim of reducing the problem to a single monovariate polynomial of 16th degree or lower. While finding the roots of a polynomial of this degree is no longer an insurmountable task, reducing the underlying system of nonlinear equations to a monovariate polynomial requires intensive computer-algebra work that must be very carefully planned to avoid the introduction of spurious roots and, with this, an increase in the degree of that polynomial. For this reason, we limit this chapter to the study of the geometric IDP of decoupled six-axis manipulators. The IDP of the most general six-revolute serial manipulator is studied in Chap. 9.

In studying the DDP of six-axis manipulators, we need not limit ourselves to a particular architecture. We thus study here the DDP of manipulators such as the one sketched in Fig. 4.9. This manipulator consists of seven rigid bodies, or links, coupled by six revolute joints. Correspondingly, we have seven frames, $\mathcal{F}_1$, $\mathcal{F}_2$, ..., $\mathcal{F}_7$, the ith frame fixed to the $(i-1)$st link, $\mathcal{F}_1$ being termed the *base frame*, because it is fixed to the base of the manipulator. Manipulators with joints of the prismatic type are simpler to study and can be treated using correspondingly simpler procedures.

A line $\mathcal{L}_i$ is associated with the axis of the ith revolute joint, and a positive direction along this line is defined arbitrarily through a unit vector $\mathbf{e}_i$. For a prismatic pair, a line $\mathcal{L}_i$ can be also defined, as a line having the direction of the pair but whose location is undefined; the analyst, then, has the freedom to locate this axis conveniently. Thus, a rotation of the ith link with respect to the $(i-1)$st link or correspondingly, of $\mathcal{F}_{i+1}$ with respect to $\mathcal{F}_i$, is totally defined by the geometry of the ith link, i.e., by the DH parameters a_i, b_i, and α_i, plus $\mathbf{e}_i$ and its associated joint variable θ_i. Then, the DH parameters and the joint variables define uniquely the posture of the manipulator. In particular, the relative position and orientation of $\mathcal{F}_{i+1}$ with respect to $\mathcal{F}_i$ is given by matrix $\mathbf{Q}_i$ and vector $\mathbf{a}_i$, respectively, which were defined in Sect. 4.2 and are displayed below for quick reference:

$$\mathbf{Q}_i = \begin{bmatrix} \cos\theta_i & -\lambda_i \sin\theta_i & \mu_i \sin\theta_i \\ \sin\theta_i & \lambda_i \cos\theta_i & -\mu_i \cos\theta_i \\ 0 & \mu_i & \lambda_i \end{bmatrix}, \quad \mathbf{a}_i = \begin{bmatrix} a_i \cos\theta_i \\ a_i \sin\theta_i \\ b_i \end{bmatrix} \tag{4.7}$$

Thus, $\mathbf{Q}_i$ and $\mathbf{a}_i$ denote, respectively, the matrix rotating $\mathcal{F}_i$ into an orientation coincident with that of $\mathcal{F}_{i+1}$ and the vector joining the origin of $\mathcal{F}_i$ with that of $\mathcal{F}_{i+1}$, directed from the former to the latter. Moreover, $\mathbf{Q}_i$ and $\mathbf{a}_i$, as given in Eq. (4.7),

are represented in $\mathcal{F}_i$ coordinates. The equations leading to the geometric model under study are known as the *displacement equations*. It is noteworthy that the problem under study is equivalent to the *input–output analysis problem* of a seven-revolute linkage with one degree of freedom and one single kinematic loop (Duffy 1980). Because of this equivalence with a *closed kinematic chain*, sometimes the displacement equations are also termed *closure equations*. These equations relate the orientation of the EE, as produced by the joint coordinates, with the prescribed orientation $\mathbf{Q}$ and the position vector $\mathbf{p}$ of the *operation point* P of the EE. That is, the orientation $\mathbf{Q}$ of the EE is obtained as a result of the six individual rotations $\{\mathbf{Q}_i\}_1^6$ about each revolute axis through an angle θ_i, in a *sequential order*, from 1 to 6. If, for example, the foregoing relations are expressed in $\mathcal{F}_1$, then

$$[\mathbf{Q}_6]_1[\mathbf{Q}_5]_1[\mathbf{Q}_4]_1[\mathbf{Q}_3]_1[\mathbf{Q}_2]_1[\mathbf{Q}_1]_1 = [\mathbf{Q}]_1 \tag{4.8a}$$

$$[\mathbf{a}_1]_1 + [\mathbf{a}_2]_1 + [\mathbf{a}_3]_1 + [\mathbf{a}_4]_1 + [\mathbf{a}_5]_1 + [\mathbf{a}_6]_1 = [\mathbf{p}]_1 \tag{4.8b}$$

Notice that the above equations require that all vectors and matrices involved be expressed *in the same coordinate frame*. However, we derived in Sect. 4.2 general expressions for $\mathbf{Q}_i$ and $\mathbf{a}_i$ in $\mathcal{F}_i$, Eqs. (4.1e) and (4.3b), respectively. It is hence convenient to represent the foregoing relations in each individual frame, which can be readily done by means of similarity transformations. Indeed, if we apply the transformations (4.5a and b) to each of $[\mathbf{a}_i]_1$ and $[\mathbf{Q}_i]_1$, respectively, we obtain $\mathbf{a}_i$ or, correspondingly, $\mathbf{Q}_i$ in $\mathcal{F}_i$. Therefore, Eq. (4.8a) becomes

$$[\mathbf{Q}_1]_1[\mathbf{Q}_2]_2[\mathbf{Q}_3]_3[\mathbf{Q}_4]_4[\mathbf{Q}_5]_5[\mathbf{Q}_6]_6 = [\mathbf{Q}]_1$$

Now for compactness, let us represent $[\mathbf{Q}]_1$ simply by $\mathbf{Q}$ and let us recall the abbreviated notation introduced in Eq. (4.1d), where $[\mathbf{Q}_i]_i$ is denoted simply by $\mathbf{Q}_i$, thereby obtaining

$$\mathbf{Q}_1\mathbf{Q}_2\mathbf{Q}_3\mathbf{Q}_4\mathbf{Q}_5\mathbf{Q}_6 = \mathbf{Q} \tag{4.9a}$$

Likewise, Eq. (4.8b) becomes

$$\mathbf{a}_1 + \mathbf{Q}_1(\mathbf{a}_2 + \mathbf{Q}_2\mathbf{a}_3 + \mathbf{Q}_2\mathbf{Q}_3\mathbf{a}_4 + \mathbf{Q}_2\mathbf{Q}_3\mathbf{Q}_4\mathbf{a}_5 + \mathbf{Q}_2\mathbf{Q}_3\mathbf{Q}_4\mathbf{Q}_5\mathbf{a}_6) = \mathbf{p} \tag{4.9b}$$

in which both sides are given in base-frame coordinates. Equations (4.9a and b) above can be cast in a more compact form if homogeneous transformations, as defined in Sect. 2.5, are now introduced. Thus, if we let $\mathbf{T}_i \equiv \{\mathbf{T}_i\}_i$ be the 4×4 matrix transforming $\mathcal{F}_{i+1}$-coordinates into $\mathcal{F}_i$-coordinates, the foregoing equations can be written in 4×4 matrix form, namely,

$$\mathbf{T}_1\mathbf{T}_2\mathbf{T}_3\mathbf{T}_4\mathbf{T}_5\mathbf{T}_6 = \mathbf{T} \tag{4.10}$$

with $\mathbf{T}$ denoting the transformation of coordinates from the end-effector frame to the base frame. Thus, $\mathbf{T}$ contains the pose of the end-effector.

In order to ease the discussion ahead, we introduce now a few definitions. A scalar, vector, or matrix expression is said to be *multilinear* in a set of vectors $\{\mathbf{v}_i\}_1^N$ if each of those vectors appears only linearly in the same expression. This does not prevent products of components of those vectors from occurring, as long as each product contains only one component of the same vector. Alternatively, we can say that the expression of interest is multilinear in the aforementioned set of vectors if and only if the partial derivative of that expression with respect to vector $\mathbf{v}_i$ is independent of $\mathbf{v}_i$, for $i = 1, \ldots, N$. For example, every matrix $\mathbf{Q}_i$ and every vector $\mathbf{a}_i$, defined in Eqs. (4.1e) and (4.3b), respectively, is linear in vector $\mathbf{x}_i$, where $\mathbf{x}_i$ is defined as

$$\mathbf{x}_i \equiv \begin{bmatrix} \cos\theta_i \\ \sin\theta_i \end{bmatrix} \tag{4.11}$$

Moreover, the product $\mathbf{Q}_1\mathbf{Q}_2\mathbf{Q}_3\mathbf{Q}_4\mathbf{Q}_5\mathbf{Q}_6$ appearing in Eq. (4.9a) is *hexalinear*, or simply, *multilinear*, in vectors $\{\mathbf{x}_i\}_1^6$. Likewise, the sum appearing in Eq. (4.9b) is multilinear in the same set of vectors. By the same token, a scalar, vector, or matrix expression is said to be *multiquadratic* in the same set of vectors if those vectors appear at most quadratically in the said expression. That is, the expression of interest may contain products of the components of all those vectors, as long as those products contain, in turn, a maximum of two components of the same vector, including the same component squared. Qualifiers like *multicubic*, *multiquartic*, etc., bear similar meanings.

Further, we partition matrix $\mathbf{Q}_i$ rowwise and columnwise, namely,

$$\mathbf{Q}_i \equiv \begin{bmatrix} \mathbf{m}_i^T \\ \mathbf{n}_i^T \\ \mathbf{o}_i^T \end{bmatrix} \equiv \begin{bmatrix} \mathbf{p}_i & \mathbf{q}_i & \mathbf{u}_i \end{bmatrix} \tag{4.12}$$

It is noteworthy that the third row $\mathbf{o}_i^T$ of $\mathbf{Q}_i$ is independent of θ_i, a fact that will be found useful in the forthcoming derivations. Furthermore, note that according to the DH notation, the unit vector $\mathbf{e}_i$ in the direction of the ith joint axis in Fig. 4.9 has $\mathcal{F}_i$-components given by

$$[\,\mathbf{e}_i\,]_i = \begin{bmatrix} 0 \\ 0 \\ 1 \end{bmatrix} \equiv \mathbf{e} \tag{4.13}$$

Henceforth, $\mathbf{e}$ is used to represent a three-dimensional array with its last component equal to unity, its other components vanishing. Thus, we have

$$\mathbf{Q}_i\mathbf{o}_i \equiv \mathbf{Q}_i^T\mathbf{u}_i = \mathbf{e} \tag{4.14a}$$

or

$$\mathbf{u}_i = \mathbf{Q}_i \mathbf{e}, \quad \mathbf{o}_i = \mathbf{Q}_i^T \mathbf{e} \tag{4.14b}$$

That is, if we regard $\mathbf{e}$ in the first of the foregoing relations as $[\,\mathbf{e}_{i+1}\,]_{i+1}$, and as $[\,\mathbf{e}_i\,]_i$ in the second relation, then, from the coordinate transformations of Eqs. (4.4a and b),

$$\mathbf{u}_i = [\,\mathbf{e}_{i+1}\,]_i, \quad \text{and} \quad \mathbf{o}_i = [\,\mathbf{e}_i\,]_{i+1} \tag{4.15}$$

4.4 The Inverse Displacement Analysis of Decoupled Manipulators

Industrial manipulators are frequently supplied with a special architecture that allows a decoupling of the positioning problem from the orientation problem. In fact, a determinant design criterion in this regard has been that the manipulator lend itself to a closed-form inverse displacement solution. Although the class of manipulators with this feature is quite broad, we will focus on a special kind, the most frequently encountered in commercial manipulators, that we have termed decoupled. Decoupled manipulators were defined in Sect. 4.2 as those whose last three joints have intersecting axes. These joints, then, constitute the *wrist* of the manipulator, which is said to be *spherical*, because when the point of intersection of the three wrist axes, C, is kept fixed, all the points of the wrist move on spheres centered at C. In terms of the DH parameters of the manipulator, in a decoupled manipulator $a_4 = a_5 = b_5 = 0$, and thus, the origins of frames 5 and 6 are coincident. All other DH parameters can assume arbitrary values. A general decoupled manipulator is shown in Fig. 4.10, where the wrist is represented as a concatenation of three revolutes with intersecting axes.

In the two subsections below, a procedure is derived for determining all the inverse displacement solutions of decoupled manipulators. In view of the decoupled architecture of these manipulators, we conduct their displacement analysis by decoupling the positioning problem from the orientation problem.

4.4.1 The Positioning Problem

We solve first the positioning problem. Let C denote the intersection of axes 4, 5, and 6, i.e., the center of the spherical wrist, and let $\mathbf{c}$ denote the position vector of this point. Apparently, the position of C is independent of joint angles θ_4, θ_5, and θ_6; hence, only the first three joints are to be considered for this analysis. The arm structure depicted in Fig. 4.11 will then be analyzed. From that figure,

$$\mathbf{a}_1 + \mathbf{Q}_1\mathbf{a}_2 + \mathbf{Q}_1\mathbf{Q}_2\mathbf{a}_3 + \mathbf{Q}_1\mathbf{Q}_2\mathbf{Q}_3\mathbf{a}_4 = \mathbf{c} \tag{4.16}$$

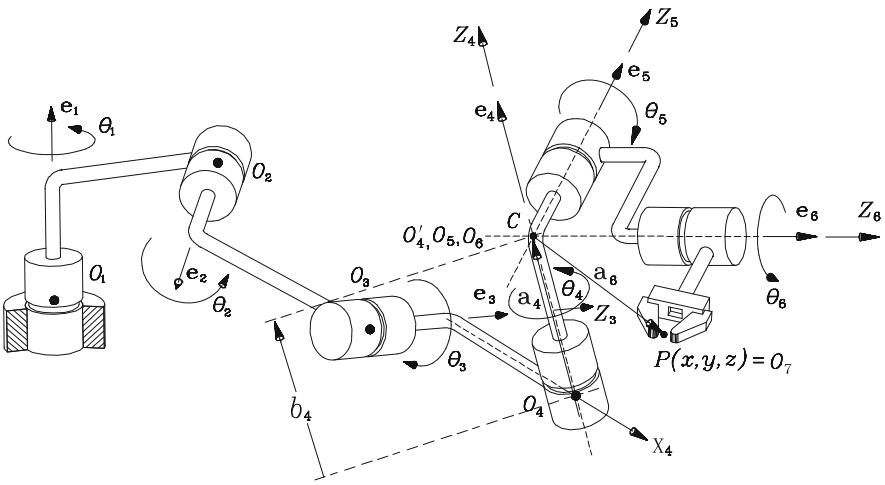

Fig. 4.10 A general 6R manipulator with decoupled architecture

where the two sides are expressed in $\mathcal{F}_1$-coordinates. This equation can be readily rewritten in the form

$$\mathbf{a}_2 + \mathbf{Q}_2\mathbf{a}_3 + \mathbf{Q}_2\mathbf{Q}_3\mathbf{a}_4 = \mathbf{Q}_1^T(\mathbf{c} - \mathbf{a}_1)$$

or if we recall Eq. (4.3d),

$$\mathbf{Q}_2(\mathbf{b}_2 + \mathbf{Q}_3\mathbf{b}_3 + \mathbf{Q}_3\mathbf{Q}_4\mathbf{b}_4) = \mathbf{Q}_1^T\mathbf{c} - \mathbf{b}_1$$

However, since we are dealing with a decoupled manipulator, we have, from Fig. 4.10,

$$\mathbf{a}_4 \equiv \mathbf{Q}_4\mathbf{b}_4 \equiv \begin{bmatrix} 0 \\ 0 \\ b_4 \end{bmatrix} \equiv b_4\mathbf{e}$$

which has been rewritten as the product of constant b_4 times the unit vector $\mathbf{e}$ defined in Eq. (4.13).

Thus, the product $\mathbf{Q}_3\mathbf{Q}_4\mathbf{b}_4$ reduces to

$$\mathbf{Q}_3\mathbf{Q}_4\mathbf{b}_4 \equiv b_4\mathbf{Q}_3\mathbf{e} \equiv b_4\mathbf{u}_3$$

with $\mathbf{u}_i$ defined in Eq. (4.14b). Hence, Eq. (4.16) leads to

$$\mathbf{Q}_2(\mathbf{b}_2 + \mathbf{Q}_3\mathbf{b}_3 + b_4\mathbf{u}_3) = \mathbf{Q}_1^T\mathbf{c} - \mathbf{b}_1 \tag{4.17}$$

Further, an expression for $\mathbf{c}$ can be derived in terms of $\mathbf{p}$, the position vector of the operation point of the EE, and $\mathbf{Q}$, namely,

$$\mathbf{c} = \mathbf{p} - \mathbf{Q}_1\mathbf{Q}_2\mathbf{Q}_3\mathbf{Q}_4\mathbf{a}_5 - \mathbf{Q}_1\mathbf{Q}_2\mathbf{Q}_3\mathbf{Q}_4\mathbf{Q}_5\mathbf{a}_6 \tag{4.18a}$$

Now, since $a_5 = b_5 = 0$, we have that $\mathbf{a}_5 = \mathbf{0}$, Eq. (4.18a) thus yielding

$$\mathbf{c} = \mathbf{p} - \mathbf{Q}\mathbf{Q}_6^T\mathbf{a}_6 \equiv \mathbf{p} - \mathbf{Q}\mathbf{b}_6 \tag{4.18b}$$

Moreover, the base coordinates of P and C, and hence, the $\mathcal{F}_1$-components of their position vectors $\mathbf{p}$ and $\mathbf{c}$, are defined as

$$[\mathbf{p}]_1 = \begin{bmatrix} x \\ y \\ z \end{bmatrix}, \quad [\mathbf{c}]_1 = \begin{bmatrix} x_C \\ y_C \\ z_C \end{bmatrix}$$

so that Eq. (4.18b) can be expanded in the form

$$\begin{bmatrix} x_C \\ y_C \\ z_C \end{bmatrix} = \begin{bmatrix} x - (q_{11}a_6 + q_{12}b_6\mu_6 + q_{13}b_6\lambda_6) \\ y - (q_{21}a_6 + q_{22}b_6\mu_6 + q_{23}b_6\lambda_6) \\ z - (q_{31}a_6 + q_{32}b_6\mu_6 + q_{33}b_6\lambda_6) \end{bmatrix} \tag{4.18c}$$

where q_{ij} is the (i, j) entry of $[\mathbf{Q}]_1$, and the positioning problem now becomes one of finding the first three joint angles necessary to position point C at a point of base coordinates x_C, y_C, and z_C. We thus have three unknowns, but we also have three equations at our disposal, namely, the three scalar equations of Eq. (4.17), and we should be able to solve the problem at hand.

In solving the foregoing system of equations, we first note that (a) the left-hand side of Eq. (4.17) appears multiplied by $\mathbf{Q}_2$; and (b) θ_2 does not appear in the right-hand side. This implies that (a) if the Euclidean norms of the two sides of that equation are equated, the resulting equation will not contain θ_2; and (b) the third scalar equation of the same equation is independent of θ_2, by virtue of the structure of the $\mathbf{Q}_i$ matrices displayed in Eq. (4.1e). Thus, we have two equations free of θ_2, which allows us to calculate the two remaining unknowns θ_1 and θ_3.

Let the Euclidean norm of the left-hand side of Eq. (4.17) be denoted by l, that of its right-hand side by r. We then have

$$\begin{aligned} l^2 &\equiv a_2^2 + b_2^2 + a_3^2 + b_3^2 + b_4^2 + 2\mathbf{b}_2^T\mathbf{Q}_3\mathbf{b}_3 + 2b_4\mathbf{b}_2^T\mathbf{u}_3 + 2\lambda_3 b_3 b_4 \\ r^2 &\equiv \|\mathbf{c}\|^2 + \|\mathbf{b}_1\|^2 - 2\mathbf{b}_1^T\mathbf{Q}_1^T\mathbf{c} \end{aligned}$$

from which it is apparent that l^2 is linear in $\mathbf{x}_3$ and r^2 is linear in $\mathbf{x}_1$, for $\mathbf{x}_i$ defined in Eq. (4.11). Upon equating l^2 with r^2, then, an equation linear in $\mathbf{x}_1$ and $\mathbf{x}_3$—not bilinear in these vectors—is readily derived, namely,

$$Ac_1 + Bs_1 + Cc_3 + Ds_3 + E = 0 \tag{4.19a}$$

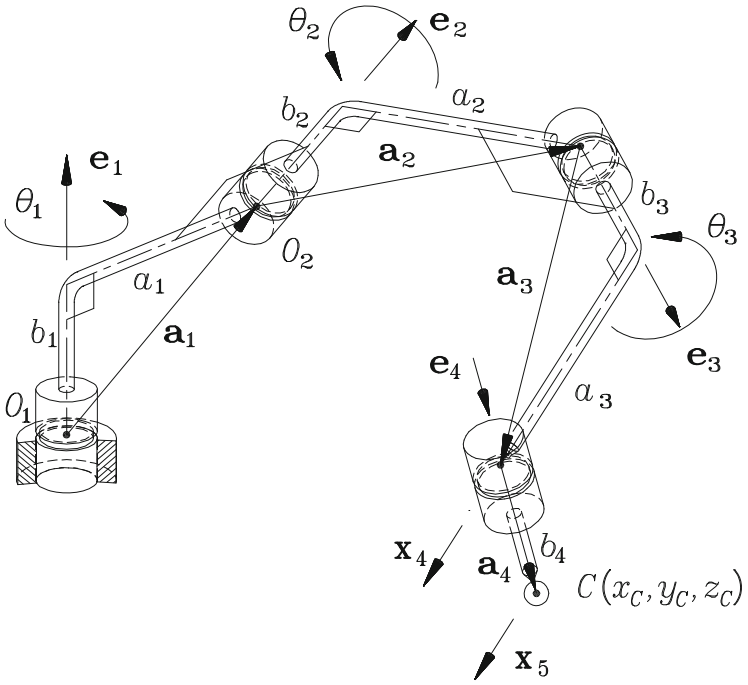

Fig. 4.11 Three-axis, serial, positioning manipulator

whose coefficients do not contain any unknown, i.e.,

$$A = 2a_1 x_C \tag{4.19b}$$

$$B = 2a_1 y_C \tag{4.19c}$$

$$C = 2a_2 a_3 - 2b_2 b_4 \mu_2 \mu_3 \tag{4.19d}$$

$$D = 2a_3 b_2 \mu_2 + 2a_2 b_4 \mu_3 \tag{4.19e}$$

$$E = a_2^2 + a_3^2 + b_2^2 + b_3^2 + b_4^2 - a_1^2 - x_C^2 - y_C^2 - (z_C - b_1)^2 + 2b_2 b_3 \lambda_2 + 2b_2 b_4 \lambda_2 \lambda_3 + 2b_3 b_4 \lambda_3 \tag{4.19f}$$

Moreover, the third scalar equation of Eq. (4.17) takes the form

$$Fc_1 + Gs_1 + Hc_3 + Is_3 + J = 0 \tag{4.20a}$$

whose coefficients, again, do not contain any unknown, as shown below:

$$F = y_C \mu_1 \tag{4.20b}$$

$$G = -x_C \mu_1 \tag{4.20c}$$

$$H = -b_4\mu_2\mu_3 \tag{4.20d}$$

$$I = a_3\mu_2 \tag{4.20e}$$

$$J = b_2 + b_3\lambda_2 + b_4\lambda_2\lambda_3 - (z_C - b_1)\lambda_1 \tag{4.20f}$$

Thus, we have derived two nonlinear equations in θ_1 and θ_3 that are linear in c_1, s_1, c_3, and s_3. Each of these equations thus defines a contour in the θ_1–θ_3 plane, their intersections determining all real solutions to the problem at hand.

Now, two well-known trigonometric identities are introduced, namely,

$$c_3 \equiv \frac{1-\tau_3^2}{1+\tau_3^2}, \quad s_3 \equiv \frac{2\tau_3}{1+\tau_3^2}, \quad \text{where } \tau_3 \equiv \tan\left(\frac{\theta_3}{2}\right) \tag{4.21}$$

Henceforth, the foregoing identities will be referred to as the *tan-half-angle identities*. We will be resorting to them throughout the book. Note that if c_i and s_i are substituted for their equivalents in terms of $\tan(\theta_i/2)$, for $i = 1, 3$, then two biquadratic polynomial equations in $\tan(\theta_1/2)$ and $\tan(\theta_3/2)$ are derived. Thus, one can eliminate one of these variables from the foregoing equations, thereby reducing the two equations to a single quartic polynomial equation in the other variable. The quartic equation thus resulting is called the *characteristic equation* of the problem at hand. Alternatively, the two above equations, Eqs. (4.19a) and (4.20a), can be solved for, say, c_1 and s_1 in terms of the data and c_3 and s_3, namely,

$$c_1 = \frac{-G(Cc_3 + Ds_3 + E) + B(Hc_3 + Is_3 + J)}{\Delta_1} \tag{4.22a}$$

$$s_1 = \frac{F(Cc_3 + Ds_3 + E) - A(Hc_3 + Is_3 + J)}{\Delta_1} \tag{4.22b}$$

with Δ_1 defined as

$$\Delta_1 = AG - FB = -2a_1\mu_1(x_C^2 + y_C^2) \tag{4.22c}$$

Note that in trajectory planning, to be studied in Chap. 6, Δ_1 can be computed *off-line*, i.e., prior to setting the manipulator into operation, for it is a function solely of the manipulator parameters and the Cartesian coordinates of a point lying on the path to be tracked. Moreover, the above calculations are possible as long as Δ_1 does not vanish. Now, Δ_1 vanishes if and only if any of the factors a_1, μ_1, and $x_C^2 + y_C^2$ does. The first two conditions are architecture-dependent, whereas the third is position-dependent. The former occur frequently in industrial manipulators, although not both at the same time. If both parameters a_1 and μ_1 vanished, then the arm would be useless to position arbitrarily a point in space. The third condition, i.e., the vanishing of $x_C^2 + y_C^2$, means that point C lies on the Z_1 axis. Now, even if neither a_1 nor μ_1 vanishes, the manipulator can be postured in a configuration at which point C lies on the Z_1 axis. Such a configuration is termed the *first*

singularity. Note, however, that with point C being located on the Z_1 axis, any motion of the first joint, with the two other joints locked, does not change the location of C. For the moment, it will be assumed that Δ_1 does not vanish, the particular cases under which it does being studied presently. Next, both sides of Eqs. (4.22a and b) are squared, the squares thus obtained are then added, and the sum is equated to 1, which leads to a quadratic equation in $\mathbf{x}_3$, namely,

$$Kc_3^2 + Ls_3^2 + Mc_3s_3 + Nc_3 + Ps_3 + Q = 0 \tag{4.23}$$

whose coefficients, after simplification, are given below:

$$K = 4a_1^2H^2 + \mu_1^2C^2 \tag{4.24a}$$

$$L = 4a_1^2I^2 + \mu_1^2D^2 \tag{4.24b}$$

$$M = 2(4a_1^2HI + \mu_1^2CD) \tag{4.24c}$$

$$N = 2(4a_1^2HJ + \mu_1^2CE) \tag{4.24d}$$

$$P = 2(4a_1^2IJ + \mu_1^2DE) \tag{4.24e}$$

$$Q = 4a_1^2J^2 + \mu_1^2E^2 - 4a_1^2\mu_1^2\rho^2 \tag{4.24f}$$

with ρ^2 defined as

$$\rho^2 \equiv x_C^2 + y_C^2$$

Upon substitution of the tan-half identities introduced in Eq. (4.21) into Eq. (4.23), a quartic equation in τ_3 is obtained, i.e.,

$$R\tau_3^4 + S\tau_3^3 + T\tau_3^2 + U\tau_3 + V = 0 \tag{4.25}$$

whose coefficients are all computable from the data. After some simplifications, these coefficients take on the forms

$$R = 4a_1^2(J - H)^2 + \mu_1^2(E - C)^2 - 4\rho^2a_1^2\mu_1^2 \tag{4.26a}$$

$$S = 4[4a_1^2I(J - H) + \mu_1^2D(E - C)] \tag{4.26b}$$

$$T = 2[4a_1^2(J^2 - H^2 + 2I^2) + \mu_1^2(E^2 - C^2 + 2D^2) - 4\rho^2a_1^2\mu_1^2] \tag{4.26c}$$

$$U = 4[4a_1^2I(H + J) + \mu_1^2D(C + E)] \tag{4.26d}$$

$$V = 4a_1^2(J + H)^2 + \mu_1^2(E + C)^2 - 4\rho^2a_1^2\mu_1^2 \tag{4.26e}$$

Furthermore, let $\{ (\tau_3)_i \}_1^4$ be the four roots of Eq. (4.25). Thus, up to four possible values of θ_3 can be obtained, namely,

$$(\theta_3)_i = 2\arctan[(\tau_3)_i], \quad i = 1, 2, 3, 4 \tag{4.27}$$

Once the four values of θ_3 are available, each of these is substituted into Eqs. (4.22a and b), which thus produce four different values of θ_1. For each value of θ_1 and θ_3, then, one value of θ_2 can be computed from the first two scalar equations of Eq. (4.17), which are displayed below:

$$A_{11}\cos\theta_2 + A_{12}\sin\theta_2 = x_C\cos\theta_1 + y_C\sin\theta_1 - a_1 \tag{4.28a}$$

$$-A_{12}\cos\theta_2 + A_{11}\sin\theta_2 = -x_C\lambda_1\sin\theta_1 + y_C\lambda_1\cos\theta_1 + (z_C - b_1)\mu_1 \tag{4.28b}$$

where

$$A_{11} \equiv a_2 + a_3\cos\theta_3 + b_4\mu_3\sin\theta_3 \tag{4.28c}$$

$$A_{12} \equiv -a_3\lambda_2\sin\theta_3 + b_3\mu_2 + b_4\lambda_2\mu_3\cos\theta_3 + b_4\mu_2\lambda_3 \tag{4.28d}$$

Thus, if A_{11} and A_{12} do not vanish simultaneously, angle θ_2 is readily computed in terms of θ_1 and θ_3 from Eqs. (4.28a and b) as

$$\cos\theta_2 = \tfrac{1}{\Delta_2}\{\, A_{11}(x_C\cos\theta_1 + y_C\sin\theta_1 - a_1) - A_{12}[-x_C\lambda_1\sin\theta_1 + y_C\lambda_1\cos\theta_1 + (z_C - b_1)\mu_1]\} \tag{4.29a}$$

$$\sin\theta_2 = \tfrac{1}{\Delta_2}\{\, A_{12}(x_C\cos\theta_1 + y_C\sin\theta_1 - a_1) + A_{11}[-x_C\lambda_1\sin\theta_1 + y_C\lambda_1\cos\theta_1 + (z_C - b_1)\mu_1]\} \tag{4.29b}$$

where Δ_2 is defined as

$$\begin{aligned}\Delta_2 &\equiv A_{11}^2 + A_{12}^2 \\ &\equiv a_2^2 + a_3^2(\cos^2\theta_3 + \lambda_2^2\sin^2\theta_3) + b_4^2\mu_3^2(\sin^2\theta_3 + \lambda_2^2\cos^2\theta_3) \\ &\quad + 2a_2a_3\cos\theta_3 + 2a_2b_4\mu_3\sin\theta_3 \\ &\quad + 2\lambda_2\mu_2(b_3 + b_4\lambda_3)(b_4\mu_3\cos\theta_3 - a_3\sin\theta_3) \\ &\quad + 2a_3b_4\mu_2^2\mu_3\sin\theta_3\cos\theta_3 + (b_3 + \lambda_3b_4)^2\mu_2^2\end{aligned} \tag{4.29c}$$

the case in which $\Delta_2 = 0$, which leads to what is termed here the *second singularity*, being discussed presently.

Takano (1985) considered the solution of the positioning problem for all possible combinations of prismatic and revolute pairs in the regional structure of a manipulator. A sketch of an intermediate P joint in a kinematic chain is displayed in Fig. 7.3. Takano found that:

1. In the case of arms containing either three revolutes, or two revolutes and one prismatic pair, with a general layout in all cases, a quartic equation in $\cos\theta_3$ is obtained;
2. in the case of one revolute and two prismatic pairs, the positioning problem was reduced to a single quadratic equation, the problem at hand thus admitting two solutions;
3. finally, for three prismatic pairs, one single linear equation was derived, the problem thus admitting a unique solution.

The Vanishing of Δ_1

In the above derivations we have assumed that neither μ_1 nor a_1 vanishes. However, if either $\mu_1 = 0$ or $a_1 = 0$, then one can readily show that Eq. (4.25) reduces to a quadratic equation, and hence, this case differs essentially from the general one. Note that one of these conditions can occur, and the second occurs indeed frequently, but both together never occur, because their simultaneous occurrence would render the axes of the first two revolutes coincident. The manipulator would thus be short of one joint for the execution of three-dimensional tasks. We thus have two cases:

1. $\mu_1 = 0$, $a_1 \neq 0$. In this case,

$$A,\ B \neq 0, \quad F = G = 0$$

Under these conditions, Eq. (4.20a) and the tan-half-angle identities given in Eq. (4.21) yield

$$(J - H)\tau_3^2 + 2I\tau_3 + (J + H) = 0$$

which thus produces two values of τ_3, namely,

$$(\tau_3)_{1,2} = \frac{-I \pm \sqrt{I^2 - J^2 + H^2}}{J - H} \tag{4.30a}$$

Once two values of θ_3 have been determined according to the above equation, θ_1 can be found using Eq. (4.19a) and the tan-half-angle identities, thereby deriving

$$(E' - A)\tau_1^2 + 2B\tau_1 + (E' + A) = 0$$

where

$$E' = Cc_3 + Ds_3 + E, \quad \tau_1 \equiv \tan\left(\frac{\theta_1}{2}\right)$$

whose roots are

$$(\tau_1)_{1,2} = \frac{-B \pm \sqrt{B^2 - E'^2 + A^2}}{E' - A} \tag{4.30b}$$

Thus, two values of θ_1 are found for each of the two values of θ_3, which results in four positioning solutions. Values of θ_2 are obtained using Eqs. (4.29a and b).

2. $a_1 = 0$, $\mu_1 \neq 0$. In this case, one has an architecture similar to that of the robot of Fig. 4.3. We have now

$$A = B = 0, \quad F, G \neq 0$$

Under the present conditions, Eq. (4.19a) reduces to

$$(E - C)\tau_3^2 + 2D\tau_3 + (E + C) = 0$$

which produces two values of τ_3, namely,

$$(\tau_3)_{1,2} = \frac{-D \pm \sqrt{D^2 - E^2 + C^2}}{E - C} \tag{4.31a}$$

With the two values of θ_3 obtained, θ_1 can be found using Eq. (4.20a) and the tan-half-angle identities to produce

$$(J' - F)\tau_1^2 + 2G\tau_1 + (J' + F) = 0$$

where

$$J' = Hc_3 + Is_3 + J, \quad \tau_1 \equiv \tan\left(\frac{\theta_1}{2}\right)$$

whose roots are

$$(\tau_1)_{1,2} = \frac{-G \pm \sqrt{G^2 - J'^2 + F^2}}{J' - F} \tag{4.31b}$$

Once again, the solution results in a cascade of two quadratic equations, one for θ_3 and one for θ_1, which yields four positioning solutions. As above, θ_2 is then determined using Eqs. (4.29a and b). Note that for the special case of the manipulator of Fig. 4.3, we have

$$a_1 = b_2 = 0, \quad \alpha_1 = \alpha_3 = 90°, \quad \alpha_2 = 0°$$

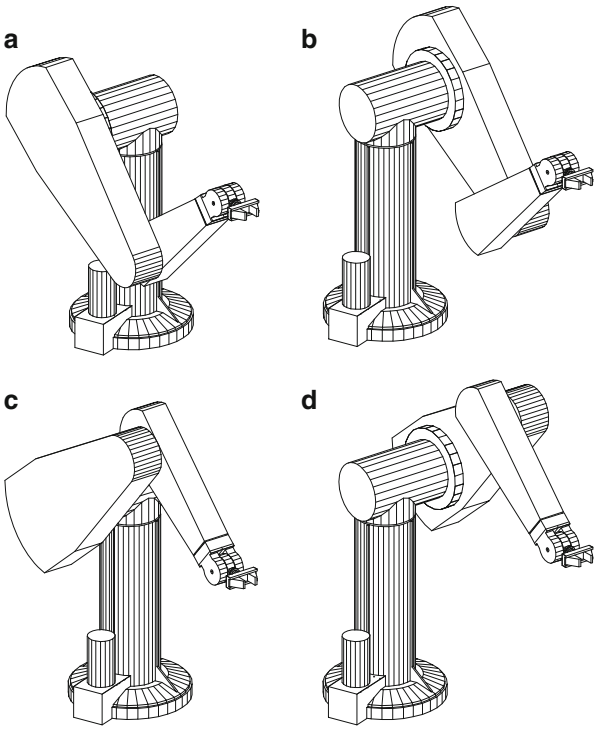

Fig. 4.12 The four arm configurations for the positioning problem of the Puma robot: (**a**, **b**) elbow down; (**a**, **c**) shoulder fore; (**c**, **d**) elbow up; (**b**, **d**) shoulder aft

and hence,

$$H = I = 0, \quad E = a_2^2 + a_3^2 + b_3^2 + b_4^2 - \left[x_C^2 + y_C^2 + (z_C - b_1)^2\right],$$
$$C = 2a_2a_3, \quad D = 2a_2b_4, \quad F = y_C, \quad G = -x_C, \quad J = b_3$$

In this case, the foregoing solutions reduce to

$$(\tau_3)_{1,2} = \frac{-D \pm \sqrt{C^2 + D^2 - E^2}}{E - C}, \quad (\tau_1)_{1,2} = \frac{x_C \pm \sqrt{x_C^2 + y_C^2 - b_3^2}}{b_3 - y_C}$$

A robot with the architecture studied here is the Puma, which is displayed in Fig. 4.12 in its four distinct postures for the same location of its wrist center. Notice that the orientation of the EE is kept constant in all four postures.

The Vanishing of Δ_2

In some instances, Δ_2, as defined in Eq. (4.29c), may vanish at a certain posture, thereby preventing the calculation of θ_2 from Eqs. (4.29a and b). This posture, termed the second singularity, occurs if both coefficients A_{11} and A_{12} of Eqs. (4.28a and b) vanish. Note that from their definitions, Eqs. (4.28c and d), these coefficients are not only position- but also architecture-dependent. Thus, an arbitrary manipulator cannot take on this configuration unless its geometric dimensions allow it. This type of singularity will be termed architecture-dependent, to distinguish it from others that are common to all robots, regardless of their particular architectures.

We can now give a geometric interpretation of the singularity at hand: First, note that the right-hand side of Eq. (4.17), from which Eqs. (4.28a and b) were derived, is identical to $\mathbf{Q}_1^T(\mathbf{c} - \mathbf{a}_1)$, which means that this expression is nothing but the $\mathcal{F}_2$-representation of the position vector of C. That is, the components of vector $\mathbf{Q}_1^T(\mathbf{c} - \mathbf{a}_1)$ are the $\mathcal{F}_2$-components of vector $\overrightarrow{O_2C}$. Therefore, the right-hand sides of Eqs. (4.28a and b) are, respectively, the X_2- and Y_2-components of vector $\overrightarrow{O_2C}$. Consequently, if $A_{11} = A_{12} = 0$, then the two foregoing components vanish and, hence, point C lies on the Z_2 axis. The first singularity thus occurs when point C lies on the axis of the first revolute, while the second occurs when the same point lies on the axis of the second revolute.

Many industrial manipulators are designed with an orthogonal architecture, which means that the angles between neighbor axes are multiples of 90°. Moreover, with the purpose of maximizing their workspace, orthogonal manipulators are designed with their second and third links of equal lengths, thereby rendering them vulnerable to this type of singularity. An architecture common to many manipulators such as the Cincinnati–Milacron, ABB, Fanuc, and others, comprises a planar two-axis layout with equal link lengths, which is capable of turning about an axis orthogonal to these two axes. This layout allows for the architecture singularity under discussion, as shown in Fig. 4.13a. The well-known Puma robot is similar to the foregoing manipulators, except that it is supplied with what is called a shoulder offset b_3, as illustrated in Fig. 4.3. This offset, however, does not prevent the Puma from attaining the same singularity, as depicted in Fig. 4.13b. Notice that in the presence of this singularity, angle θ_2 is undetermined, but θ_1 and θ_3 are determined in the case of the Puma robot. However, in the presence of the singularity of Fig. 4.13a, neither θ_1 nor θ_2 are determined; only θ_3 of the arm structure is determined.

Example 4.4.1. A manipulator with a common orthogonal architecture is displayed in Fig. 4.14 in an arbitrary configuration. The arm architecture of this manipulator has the DH parameters shown below:

$$a_1 = a_3 = 0, \quad b_1 = b_2 = b_3 = 0, \quad \alpha_1 = 90°, \quad \alpha_2 = 0°, \quad \alpha_3 = 90°$$

Find its inverse kinematics solutions.

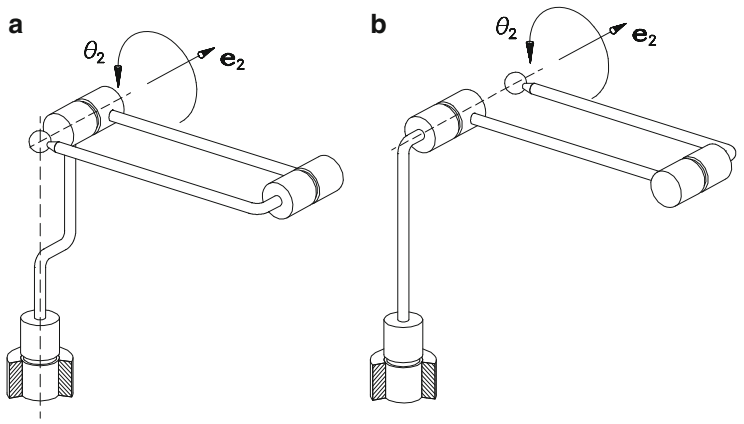

Fig. 4.13 Architecture-dependent singularities of (**a**) the Cincinnati–Milacron and (**b**) the Puma robots

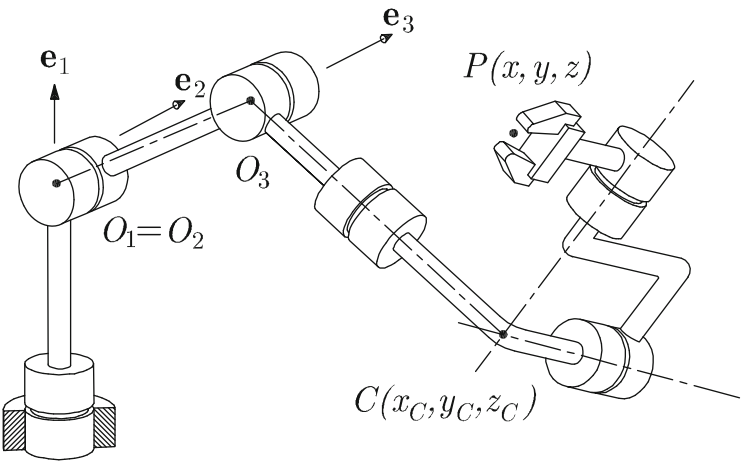

Fig. 4.14 An orthogonal decoupled manipulator

Solution: A common feature of this architecture is that it comprises $a_2 = b_4$. In the present discussion, however, the latter feature need not be included, and hence, the result that follows applies even in its absence. In this case, coefficients C, D, and E take on the forms

$$C = 0, \quad D = 2a_2b_4, \quad E = a_2^2 + b_4^2 - \|\mathbf{c}\|^2$$

Hence,

$$C = H = I = J = 0$$

and so

$$J' = 0, \quad F = y_C, \quad G = -x_C$$

The radical of Eq. (4.31b) reduces to $x_C^2 + y_C^2$. Thus,

$$\tan\left(\frac{\theta_1}{2}\right) = \frac{x_C \pm \sqrt{x_C^2 + y_C^2}}{-y_C} \equiv \frac{-1 \pm \sqrt{1 + (y_C/x_C)^2}}{y_C/x_C} \tag{4.32a}$$

Now we recall the relation between $\tan(\theta_1/2)$ and $\tan\theta_1$, namely,

$$\tan\left(\frac{\theta_1}{2}\right) \equiv \frac{-1 \pm \sqrt{1 + \tan^2\theta_1}}{\tan\theta_1} \tag{4.32b}$$

Upon comparison of Eqs. (4.32a) and (4.32b), it is apparent that

$$\theta_1 = \arctan\left(\frac{y_C}{x_C}\right)$$

a result that can be derived geometrically for this simple arm architecture. Given that the arctan(·) function is double-valued, its two values differing in 180°, we obtain here, again, two values for θ_1. On the other hand, θ_3 is calculated from Eq. (4.31a) as

$$(\tau_3)_{1,2} = \frac{-2a_2b_4 \pm \sqrt{4a_2^2b_4^2 - (a_2^2 + b_4^2 - \|\mathbf{c}\|^2)^2}}{a_2^2 + b_4^2 - \|\mathbf{c}\|^2}$$

thereby obtaining two values of θ_3. As a consequence, the inverse positioning problem of this arm architecture admits four solutions as well. These solutions give rise to two pairs of arm postures that are usually referred to as *elbow-up* and *elbow-down*.

Example 4.4.2. Find all real inverse displacement solutions of the manipulator shown in Fig. 4.15, when point C of its end-effector has the base coordinates $C(0, 2a, -a)$.

Solution: The Denavit–Hartenberg parameters of this manipulator are derived from Fig. 4.16, where the coordinate frames involved are indicated. In defining the coordinate frames of that figure, the Denavit–Hartenberg notation was followed, with Z_4 defined, arbitrarily, as parallel to Z_3. From Fig. 4.16, then, we have

$$a_1 = a_2 = a_3 = b_2 = b_3 = a, \quad b_1 = b_4 = 0, \quad \alpha_1 = \alpha_2 = 90^\circ, \quad \alpha_3 = 0^\circ$$

One inverse displacement solution can be readily inferred from the geometry of Fig. 4.16. For illustration purposes, and in order to find all other inverse kinematic

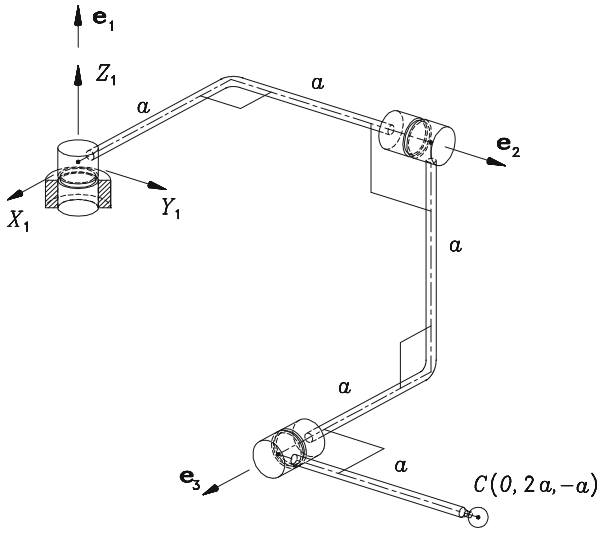

Fig. 4.15 An orthogonal *RRR* manipulator

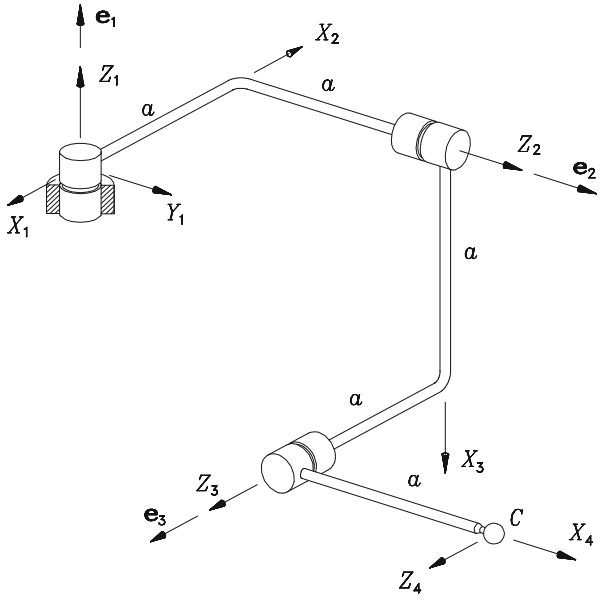

Fig. 4.16 The coordinate frames of the orthogonal *RRR* manipulator

solutions, we will use the procedure derived above. To this end, we first proceed to calculate the coefficients of the quartic polynomial equation, Eq. (4.25), which are given, nevertheless, in terms of coefficients $K, \ldots, Q$ of Eqs. (4.24a–f). These

coefficients are given, in turn, in terms of coefficients $A, \ldots, J$ of Eqs. (4.19b–f) and (4.20b–f). We then proceed to calculate all the necessary coefficients in the proper order:

$$A = 0, \quad B = 4a^2, \quad C = D = -E = 2a^2$$
$$F = 2a, \quad G = H = 0, \quad I = J = a$$

Moreover,

$$K = 4a^4, \quad L = 8a^4, \quad M = 8a^4, \quad N = -8a^4, \quad P = 0, \quad Q = -8a^4,$$

The set of coefficients sought thus reduces to

$$R = K - N + Q = 4a^4$$
$$S = 2(P - M) = -16a^4$$
$$T = 2(Q + 2L - K) = 8a^4$$
$$U = 2(M + P) = 16a^4$$
$$V = K + N + Q = -12a^4$$

which leads to a quartic equation, namely,

$$\tau_3^4 - 4\tau_3^3 + 2\tau_3^2 + 4\tau_3 - 3 = 0$$

with four real roots:

$$(\tau_3)_1 = (\tau_3)_2 = 1, \quad (\tau_3)_3 = -1, \quad (\tau_3)_4 = 3$$

These roots yield the θ_3 values that follow:

$$(\theta_3)_1 = (\theta_3)_2 = 90°, \quad (\theta_3)_3 = -90°, \quad (\theta_3)_4 = 143.13°$$

The quartic polynomial thus admits one double root, which means that at the configurations resulting from this root, two solutions meet, thereby producing a *singularity*, an issue that is discussed in Sect. 5.4. Below, we calculate the remaining angles for each solution: Angle θ_1 is computed from relations (4.22a–c), where $\Delta_1 = -8a^3$.

The first two roots, $(\theta_3)_1 = (\theta_3)_2 = 90°$, yield $c_3 = 0$ and $s_3 = 1$. Hence, Eqs. (4.22a and b) lead to

$$c_1 = \frac{B(I + J)}{\Delta_1} = \frac{4a^2(a + a)}{-8a^3} = -1$$
$$s_1 = \frac{F(D + E)}{\Delta_1} = \frac{2a(2a^2 - 2a^2)}{-8a^3} = 0$$

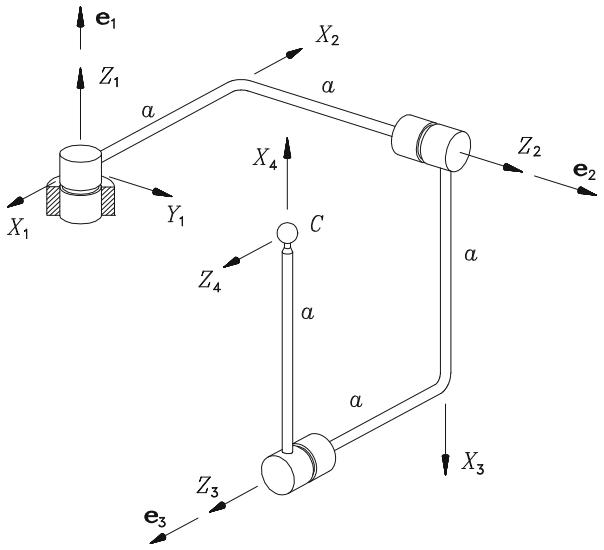

Fig. 4.17 Manipulator configuration for $C(0,\ a,\ 0)$

and hence,

$$(\theta_1)_1 = (\theta_1)_2 = 180^\circ$$

With θ_1 known, θ_2 is computed from the first two of Eqs. (4.17), namely,

$$c_2 = 0, \quad s_2 = -1$$

and hence,

$$(\theta_2)_1 = (\theta_2)_2 = -90^\circ$$

The remaining roots are treated likewise, thereby obtaining

$$(\theta_1)_3 = 90^\circ, \quad (\theta_2)_3 = 0, \quad (\theta_1)_4 = 143.13^\circ, \quad (\theta_2)_4 = 0$$

It is noteworthy that the architecture of this manipulator does not allow for the second singularity, associated with $\Delta_2 = 0$.

Example 4.4.3. For the same manipulator of Example 4.4.2, find all real inverse displacement solutions when point C of its end-effector has the base coordinates $C(0,\ a,\ 0)$, as displayed in Fig. 4.17.

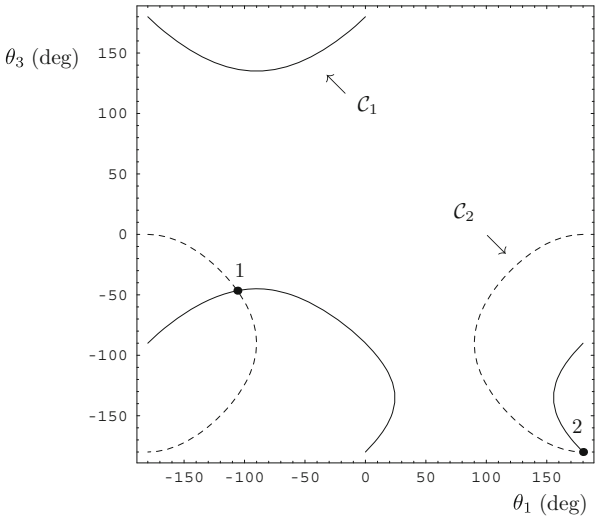

Fig. 4.18 Contours producing the two real solutions for Example 4.4.3

Solution: In this case, one obtains, successively,

$$A = 0, \quad B = C = D = E = 2a^2,$$
$$F = a, \quad G = 0 \quad H = 0, \quad I = J = a$$
$$K = 4a^4, L = M = N = 8a^4, \quad P = 16a^4, \quad Q = 4a^4$$
$$R = 0, \quad S = 16a^4, \quad T = 32a^4, \quad U = 48a^4, \quad V = 16a^4$$

Moreover, for this case, the quartic Eq. (4.23) degenerates into a cubic equation, namely,

$$\tau_3^3 + 2\tau_3^2 + 3\tau_3 + 1 = 0$$

whose roots are readily found as

$$(\tau_3)_1 = -0.43016, \quad (\tau_3)_{2,3} = -0.78492 \pm j1.30714$$

where j is the imaginary unit, i.e., $j \equiv \sqrt{-1}$. That is, only one real solution is obtained, namely, $(\theta_3)_1 = -46.551°$. However, shown in Fig. 4.17 is a quite symmetric posture of this manipulator at the given position of point C of its end-effector, which does not correspond to the real solution obtained above. In fact, the solution yielding the posture of Fig. 4.17 disappeared because of the use of the quartic polynomial equation in $\tan(\theta_3/2)$. Note that if the two contours derived from Eqs. (4.19a) and (4.20a) are plotted, as in Fig. 4.18, their intersections yield the two real roots, including the one leading to the posture of Fig. 4.17.

The explanation of how the fourth root of the quartic equation disappeared is given below: Let us write the quartic polynomial in full, with a "small" leading coefficient ϵ, namely,

$$\epsilon\tau_3^4 + \tau_3^3 + 2\tau_3^2 + 3\tau_3 + 1 = 0$$

Upon dividing both sides of the foregoing equation by τ_3^4, we obtain

$$\epsilon + \frac{1}{\tau_3} + \frac{2}{\tau_3^2} + \frac{3}{\tau_3^3} + \frac{1}{\tau_3^4} = 0$$

Apparently, the original equation is satisfied as $\epsilon \to 0$ if and only if $\tau_3 \to \pm\infty$, i.e, if $\theta_3 = 180°$. The missing root is, hence, $(\theta_3)_4 = \pi$. The remaining angles are readily calculated as

$$(\theta_1)_1 = -105.9°, \quad (\theta_2)_1 = -149.35°, \quad (\theta_1)_4 = 180°, \quad (\theta_2)_4 = -90°$$

4.4.2 The Orientation Problem

Now the orientation inverse displacement problem is first formulated, then solved. This problem consists in determining the wrist angles that will produce a prescribed orientation of the end-effector. The orientation, in turn, is given in terms of the rotation matrix $\mathbf{Q}$ taking the end-effector from its home attitude to its current one. Alternatively, the orientation can be given by the natural invariants of the rotation matrix, vector $\mathbf{e}$ and angle ϕ. In any event, all nine components of matrix $\mathbf{Q}$ are known in $\mathcal{F}_1$. It is convenient to assume a columnwise partitioning of $[\mathbf{Q}]_1$ similar to that of $\mathbf{Q}_i (\equiv [\mathbf{Q}_i]_i)$ displayed in Eq. (4.12), namely,

$$[\mathbf{Q}]_1 = \begin{bmatrix} \mathbf{p} & \mathbf{q} & \mathbf{u} \end{bmatrix} \tag{4.33}$$

Without loss of generality it can be assumed that Z_7 is defined parallel to Z_6—as the chain is open, the analyst is free to define Z_7 at will. From Definition 2.2.1, then $[u]1 = [e7]1 = [e6]1$, and $\mathbf{e}_6$ included in Fig. 4.19. Moreover, since θ_1, θ_2, and θ_3 are available, $\mathbf{Q}_1$, $\mathbf{Q}_2$, and $\mathbf{Q}_3$ become data for this problem. One now has the general layout of Fig. 4.19, where angles $\{\theta_i\}_4^6$ are to be determined from the problem data, which are in this case the orientation of the end-effector and the architecture of the wrist; the latter is defined by angles α_4 and α_5, neither of which can be either 0 or π.

Now, since the orientation of the end-effector is given, the components of $[\mathbf{e}_6]_1$ are known, but they will be needed in frame 4. A coordinate transformation from frame 1 to frame 4 can be readily implemented by resorting to the transformation given in Eq. (4.6a):

$$[\mathbf{e}_6]_4 = (\mathbf{Q}_1\mathbf{Q}_2\mathbf{Q}_3)^T[\mathbf{e}_6]_1 \equiv (\mathbf{Q}_1\mathbf{Q}_2\mathbf{Q}_3)^T[\mathbf{u}]_1 \tag{4.34}$$

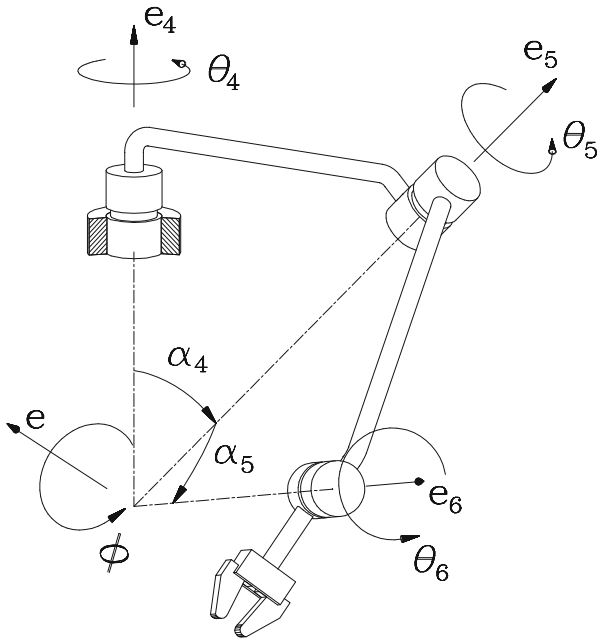

Fig. 4.19 General architecture of a spherical wrist

Let the components of $[\,\mathbf{e}_6\,]_4$, all of them known, be defined as

$$[\,\mathbf{e}_6\,]_4 = \begin{bmatrix} \xi \\ \eta \\ \zeta \end{bmatrix} \tag{4.35}$$

Moreover, based on the first of Eqs. (4.15), the components of vector $\mathbf{e}_5$ in $\mathcal{F}_4$ are nothing but the entries of the third column of matrix $\mathbf{Q}_4$, i.e.,

$$[\,\mathbf{e}_5\,]_4 = \begin{bmatrix} \mu_4 \sin\theta_4 \\ -\mu_4 \cos\theta_4 \\ \lambda_4 \end{bmatrix} \tag{4.36}$$

Furthermore, vectors $\mathbf{e}_5$ and $\mathbf{e}_6$ make an angle α_5, and hence,

$$\mathbf{e}_6^T \mathbf{e}_5 = \lambda_5 \quad \text{or} \quad [\,\mathbf{e}_6\,]_4^T [\,\mathbf{e}_5\,]_4 = \lambda_5 \tag{4.37}$$

Upon substitution of Eqs. (4.35) and (4.36) into Eq. (4.37), we obtain

$$\xi\mu_4 \sin\theta_4 - \eta\mu_4 \cos\theta_4 + \zeta\lambda_4 = \lambda_5 \tag{4.38}$$

which can be readily transformed, with the aid of the tan-half-angle identities, into a quadratic equation in $\tau_4 \equiv \tan(\theta_4/2)$, namely,

$$(\lambda_5 - \eta\mu_4 - \zeta\lambda_4)\tau_4^2 - 2\xi\mu_4\tau_4 + (\lambda_5 + \eta\mu_4 - \zeta\lambda_4) = 0 \tag{4.39}$$

its two roots being given by

$$\tau_4 = \frac{\xi\mu_4 \pm \sqrt{(\xi^2 + \eta^2)\mu_4^2 - (\lambda_5 - \zeta\lambda_4)^2}}{\lambda_5 - \zeta\lambda_4 - \eta\mu_4} \tag{4.40}$$

Note that the two foregoing roots are real as long as the radical is positive, the two roots merging into a single one when the radical vanishes. Thus, a negative radical means an attitude of the EE that is not feasible with the wrist. It is noteworthy that a three-revolute spherical wrist is kinematically equivalent to a spherical joint. However, the spherical wrist differs essentially from a spherical joint in that the latter has, kinematically, an unlimited workspace—a physical spherical joint, of course, has a limited workspace by virtue of its mechanical construction—and can orient a rigid body arbitrarily. Therefore, the workspace $\mathcal{W}$ of the wrist is not unlimited, but rather defined by the set of values of ξ, η, and ζ that satisfy the two relations shown below:

$$\xi^2 + \eta^2 + \zeta^2 = 1 \tag{4.41a}$$

$$f(\xi, \eta, \zeta) \equiv (\xi^2 + \eta^2)\mu_4^2 - (\lambda_5 - \zeta\lambda_4)^2 \geq 0 \tag{4.41b}$$

In view of condition (4.41a), however, relation (4.41b) simplifies to an inequality in ζ alone, namely,

$$F(\zeta) \equiv \zeta^2 - 2\lambda_4\lambda_5\zeta - (\mu_4^2 - \lambda_5^2) \leq 0 \tag{4.42}$$

As a consequence,

1. $\mathcal{W}$ is a region of the unit sphere $\mathcal{S}$ centered at the origin of the three-dimensional space;
2. $\mathcal{W}$ is bounded by the two *parallels* given by the roots of $F(\zeta) = 0$ on the sphere;
3. the wrist attains its singular configurations along the two foregoing parallels.

In order to gain more insight on the shape of the workspace $\mathcal{W}$, let us look at the boundary defined by $F(\zeta) = 0$. Upon setting $F(\zeta)$ to zero, we obtain a quadratic equation in ζ, whose two roots can be readily found to be

$$\zeta_{1,2} = \lambda_4\lambda_5 \pm |\mu_4\mu_5| \tag{4.43}$$

which thus defines two planes, Π_1 and Π_2, parallel to the ξ–η plane of the three-dimensional space, intersecting the ζ-axis at ζ_1 and ζ_2, respectively. Thus, the workspace $\mathcal{W}$ of the spherical wrist at hand is that region of the surface of the unit

sphere $\mathcal{S}$ contained between the two parallels defined by Π_1 and Π_2. For example, a common wrist design involves an orthogonal architecture, i.e., $\alpha_4 = \alpha_5 = 90°$. For such wrists,

$$\zeta_{1,2} = \pm 1$$

and hence, orthogonal wrists become singular when $[\mathbf{e}_6]_4 = [0, 0, \pm 1]^T$, i.e., when the fourth and the sixth axes are aligned. Thus, the workspace of orthogonal spherical wrists is the whole surface of the unit sphere centered at the origin, the singularity curve thus degenerating into two points, namely, the two intersections of this sphere with the ζ-axis. If one views $\zeta = 0$ as the equatorial plane, then the two singularity points of the workspace are the poles.

An alternative design is the so-called *three-roll wrist* of some Cincinnati-Milacron robots, with $\alpha_4 = \alpha_5 = 120°$, thereby leading to $\lambda_4 = \lambda_5 = -1/2$ and $\mu_4 = \mu_5 = \sqrt{3}/2$. For this wrist, the two planes Π_1 and Π_2 are found below: First, we note that with the foregoing architecture,

$$\zeta_{1,2} = 1, -\frac{1}{2}$$

and hence, the workspace of this wrist is the part of the surface of the unit sphere $\mathcal{S}$ that lies between the planes Π_1 and Π_2 parallel to the ξ-η plane, intersecting the ζ-axis at $\zeta_1 = 1$ and $\zeta_2 = -1/2$, respectively. Hence, if $\zeta = 0$ is regarded as the equatorial plane, then the points of the sphere $\mathcal{S}$ that are outside of the workspace of this wrist are those lying at a latitude smaller than $-30°$. The singularity points are thus the north pole and those lying on the parallel of latitude $-30°$.

Once θ_4 is calculated from the two foregoing values of τ_4, if these are real, angle θ_5 is obtained uniquely for each value of θ_4, as explained below: First, Eq. (4.9a) is rewritten in a form in which the data are collected in the right-hand side, which produces

$$\mathbf{Q}_4\mathbf{Q}_5\mathbf{Q}_6 = \mathbf{R} \tag{4.44a}$$

with $\mathbf{R}$ defined as

$$\mathbf{R} = \mathbf{Q}_3^T\mathbf{Q}_2^T\mathbf{Q}_1^T\mathbf{Q} \tag{4.44b}$$

Moreover, let the entries of $\mathbf{R}$ in the fourth coordinate frame be given as

$$[\mathbf{R}]_4 = \begin{bmatrix} r_{11} & r_{12} & r_{13} \\ r_{21} & r_{22} & r_{23} \\ r_{31} & r_{32} & r_{33} \end{bmatrix}$$

Expressions for θ_5 and θ_6 can be readily derived by solving first for $\mathbf{Q}_5$ from Eq. (4.44a), namely,

$$\mathbf{Q}_5 = \mathbf{Q}_4^T\mathbf{R}\mathbf{Q}_6^T \tag{4.45}$$

Now, by virtue of the form of the $\mathbf{Q}_i$ matrices, as appearing in Eq. (4.1e), it is apparent that the third row of $\mathbf{Q}_i$ does not contain θ_i. Hence, the third column of the matrix product of Eq. (4.45) is independent of θ_6. Thus, two equations for θ_5 are obtained by equating the first two components of the third columns of that equation, thereby obtaining

$$\begin{aligned} \mu_5 s_5 &= (\mu_6 r_{12} + \lambda_6 r_{13})c_4 + (\mu_6 r_{22} + \lambda_6 r_{23})s_4 \\ -\mu_5 c_5 &= -\lambda_4(\mu_6 r_{12} + \lambda_6 r_{13})s_4 + \lambda_4(\mu_6 r_{22} + \lambda_6 r_{23})c_4 + \mu_4(\mu_6 r_{32} + \lambda_6 r_{33}) \end{aligned}$$

which thus yield a unique value of θ_5 for every value of θ_4. Finally, with θ_4 and θ_5 known, it is a simple matter to calculate θ_6. This is done upon solving for $\mathbf{Q}_6$ from Eq. (4.44a), i.e.,

$$\mathbf{Q}_6 = \mathbf{Q}_5^T \mathbf{Q}_4^T \mathbf{R}$$

and if the partitioning (4.12) of $\mathbf{Q}_i$ is now recalled, a useful vector equation is derived, namely,

$$\mathbf{p}_6 = \mathbf{Q}_5^T \mathbf{Q}_4^T \mathbf{r}_1 \tag{4.46}$$

where $\mathbf{r}_1$ is the first column of $\mathbf{R}$. Let $\mathbf{w}$ denote the product $\mathbf{Q}_4^T \mathbf{r}_1$, i.e.,

$$\mathbf{w} \equiv \mathbf{Q}_4^T \mathbf{r}_1 \equiv \begin{bmatrix} r_{11}c_4 + r_{21}s_4 \\ -\lambda_4(r_{11}s_4 - r_{21}c_4) + \mu_4 r_{31} \\ \mu_4(r_{11}s_4 - r_{21}c_4) + \lambda_4 r_{31} \end{bmatrix}$$

Hence,

$$\mathbf{Q}_5^T \mathbf{Q}_4^T \mathbf{r}_1 \equiv \begin{bmatrix} w_1 c_5 + w_2 s_5 \\ \lambda_5(-w_1 s_5 + w_2 c_5) + w_3 \mu_5 \\ \mu_5(w_1 s_5 - w_2 c_5) + w_3 \lambda_5 \end{bmatrix}$$

in which w_i denotes the ith component of $\mathbf{w}$. Hence, c_6 and s_6 are determined from the first two scalar equations of Eq. (4.46), namely,

$$\begin{aligned} c_6 &= w_1 c_5 + w_2 s_5 \\ s_6 &= -w_1 \lambda_5 s_5 + w_2 \lambda_5 c_5 + w_3 \mu_5 \end{aligned}$$

thereby deriving a unique value of θ_6 for every pair of values (θ_4, θ_5). In summary, then, two values of θ_4 have been determined, each value determining, in turn, one single corresponding set of θ_5 and θ_6 values. Therefore, there are two sets of solutions for the orientation problem under study, which lead to two corresponding

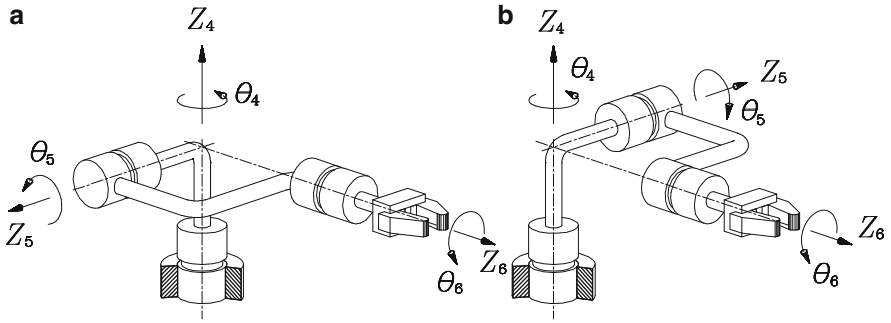

Fig. 4.20 The two configurations of a three-axis spherical wrist

wrist postures. The two distinct postures of an orthogonal three-revolute spherical wrist for a given orientation of its EE are displayed in Fig. 4.20.

When combined with the four postures of a decoupled manipulator leading to one and the same location of its wrist center—positioning problem—a maximum of eight possible combinations of joint angles for a single pose of the end-effector of a decoupled manipulator are found.

Example 4.4.4. A three-roll wrist is mounted on the orthogonal manipulator of Fig. 4.17, as this finds itself at the posture shown in the same figure, so that the center of the wrist coincides with point C of the orthogonal manipulator. The assembly is depicted in Fig. 4.21, which shows axis Z_4 parallel to Z_1. Moreover, the EE is desired to attain the orientation given by matrix $\mathbf{Q}$, defined below in $\mathcal{F}_1$-coordinates:

$$\mathbf{Q} = \begin{bmatrix} -1/3 & -2/3 & 2/3 \\ -2/3 & -1/3 & -2/3 \\ 2/3 & -2/3 & -1/3 \end{bmatrix}$$

Find the inverse-displacement solutions of the wrist that corresponds to the fourth solution found in Example 4.4.3 for the first three joint angles. Moreover, these angles can also be found from Fig. 4.21 by inspection.

Furthermore, to complete the DH parameters, Z_7 is defined as passing through C and P, in the directions from the former to the latter, which is assumed to yield an angle $\alpha_6 = 0$. The three-roll wrist is illustrated in Fig. 4.22.

Solution: As the reader can readily verify, the arm inverse-displacement solution displayed in Fig. 4.21 is

$$\theta_1 = \pi, \quad \theta_2 = -\frac{\pi}{2}, \quad \theta_3 = \pi$$

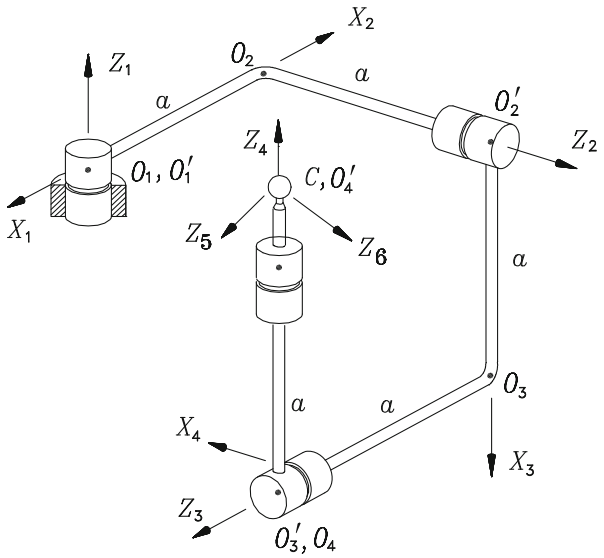

Fig. 4.21 The coordinate frames of the orthogonal $RRRR$ manipulator

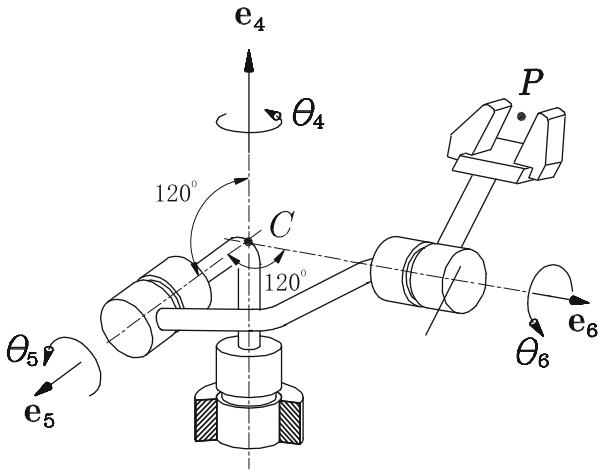

Fig. 4.22 A representation of the kinematic chain of the Cincinnati–Milacron three-roll wrist

Further, given the wrist architecture,

$$\lambda_4 = \lambda_5 = -\frac{1}{2}, \quad \mu_4 = \mu_5 = \frac{\sqrt{3}}{2}$$

and, in light of the value of α_6 given above,

$$\lambda_6 = 1, \quad \mu_6 = 0$$

Now we need $\mathbf{e}_5$ and $\mathbf{e}_6$ in $\mathcal{F}_4$; we have $[\,\mathbf{e}_5\,]_4$ displayed in Eq. (4.36), and hence, $[\,\mathbf{e}_5]_4 = [\,\sqrt{3}s\theta_4,\, -\sqrt{3}c\theta_4,\, -1\,]^T/2$. Moreover, $[\,\mathbf{e}_6\,]_1$ is simply the third column of $\mathbf{Q}$, namely, $[\,\mathbf{e}_6\,]_1 = [\,2/3,\, -2/3,\, -1/3\,]^T$. In order to bring the components of $\mathbf{e}_6$ into $\mathcal{F}_4$, a coordinate transformation is needed. This transformation is implemented by means of the transpose of the rotation matrix $\mathbf{Q}_{123} \equiv \mathbf{Q}_1\mathbf{Q}_2\mathbf{Q}_3$ that carries $\mathcal{F}_1$ into $\mathcal{F}_4$. This matrix is most simply found from Definition 2.2.1 as applied to the foregoing frames, and upon inspection of Fig. 4.21. Therefore,

$$\mathbf{Q}_{123} = \mathbf{Q}_1\mathbf{Q}_2\mathbf{Q}_3 = \begin{bmatrix} 0 & -1 & 0 \\ 1 & 0 & 0 \\ 0 & 0 & 1 \end{bmatrix}$$

Hence,

$$[\,\mathbf{e}_6\,]_4 = \mathbf{Q}_1\mathbf{Q}_2\mathbf{Q}_3^T[\,\mathbf{e}_6\,]_1 = \begin{bmatrix} 0 & 1 & 0 \\ -1 & 0 & 0 \\ 0 & 0 & 1 \end{bmatrix} \begin{bmatrix} 2/3 \\ -2/3 \\ -1/3 \end{bmatrix} = \begin{bmatrix} 2/3 \\ 2/3 \\ -1/3 \end{bmatrix}$$

which thus leads to the equation for θ_4:

$$2 + \sqrt{3}\sin\theta_4 - \sqrt{3}\cos\theta_4 = 0$$

Upon application of the tan-half identities to the above equation, a quadratic equation in $\tau_4 = \tan(\theta_4/2)$ is derived, namely,

$$2 + 2\,{\tau_4}^2 + 2\sqrt{3}\tau_4 + \sqrt{3} + \sqrt{3}{\tau_4}^2 = 0$$

whose two roots lead to the two values of θ_4 given below:

$$\theta_{4,1} = -9.7356103370^\circ, \quad \theta_{4,2} = 80.2643896700^\circ$$

Further, matrix $\mathbf{R}$ of Eq. (4.44b) is obtained as

$$\mathbf{R} = \begin{bmatrix} 2/3 & 1/3 & 2/3 \\ -1/3 & -2/3 & 2/3 \\ 2/3 & -2/3 & -1/3 \end{bmatrix}$$

Upon substitution of the above expression into Eq. (4.45), expressions for c_5 and s_5 are obtained in terms of θ_4:

$$c_5 = \frac{\sqrt{3}}{9}\left(-2\sin\theta_4 + 2\cos\theta_4 + \sqrt{3}\right)$$

and

$$s_5 = \frac{4\sqrt{3}}{9}(\cos\theta_4 + \sin\theta_4)$$

If now each of the two values obtained above for θ_4 is substituted in the above equation, the corresponding values for θ_5 are obtained as

$$\theta_{5,1} = 38.9424412300^\circ, \quad \theta_{5,2} = -38.9424412600^\circ$$

Finally, the product $\mathbf{Q}_5^T\mathbf{Q}_4^T\mathbf{R}$ is computed, then equated to $\mathbf{Q}_6$. The (1, 1) and (2, 1) entries of the foregoing product yield $\cos\theta_6$ and $\sin\theta_6$, respectively, as per Eq. (4.46). Two values are thus obtained for θ_6, one for each pair of (θ_4, θ_5) values:

$$\theta_{6,1} = -39.4804916600^\circ, \quad \theta_{6,2} = -110.0092709000^\circ$$

thereby completing the inverse-displacement solutions for the given orientation problem.

4.5 Exercises

4.1 Shown in Fig. 10.3 is the kinematic chain of one of the six-dof legs of a flight simulator, whose architecture is defined by the HD parameters of Table 10.1. In the flight simulator, $\mathcal{M}$ is the moving platform, to which an aircraft cockpit is rigidly attached. The six-dof motion of $\mathcal{M}$ is controlled by means of the six hydraulic cylinders identical to that indicated in Fig. 10.3 as a prismatic joint. Find all inverse displacement solutions of this manipulator, relating the pose of $\mathcal{M}$ with all the joint variables.

4.2 Modify the solution procedure of Sect. 4.4 to obtain all the postures of a PRR manipulator that give the same EE pose, and show that this problem leads to a quartic polynomial equation.

4.3 Repeat Exercise 4.2 as pertaining to a PRP manipulator.

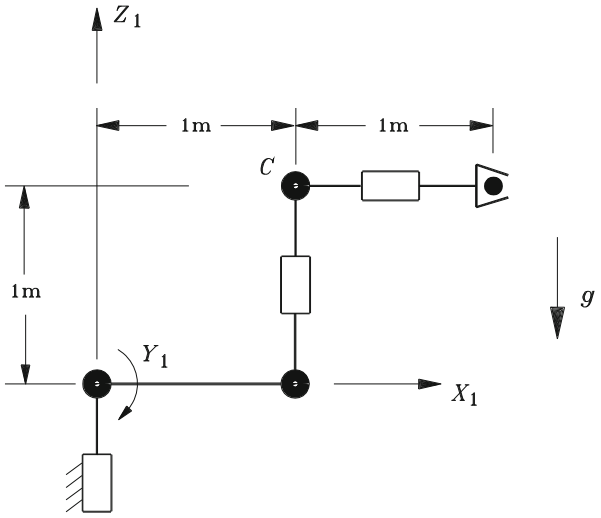

Fig. 4.23 A six-revolute robot holding a heavy tool

Fig. 4.24 ABB-IRB 1000 robotic manipulator

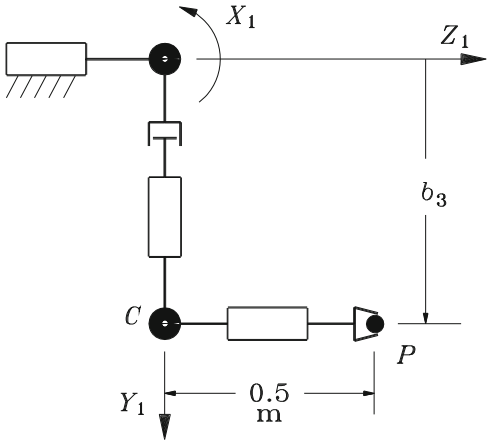

4.4 The manipulator appearing in Fig. 4.23 is of the orthogonal type, with a decoupled, spherical wrist, and a regional structure consisting of two parallel axes and one axis perpendicular to these two. Find all inverse kinematics solutions for arbitrary poses of the EE of this manipulator.

4.5 Similar to the manipulator of Fig. 4.23, that of Fig. 4.24 is of the orthogonal, decoupled type, except that the latter has a prismatic pair. For an arbitrary pose of its EE, find all inverse displacement solutions of this manipulator.

4.6 Derive expressions for the angle of rotation and the unit vector parallel to the axis of rotation of matrices $\mathbf{Q}_i$, as introduced in Sect. 4.2.

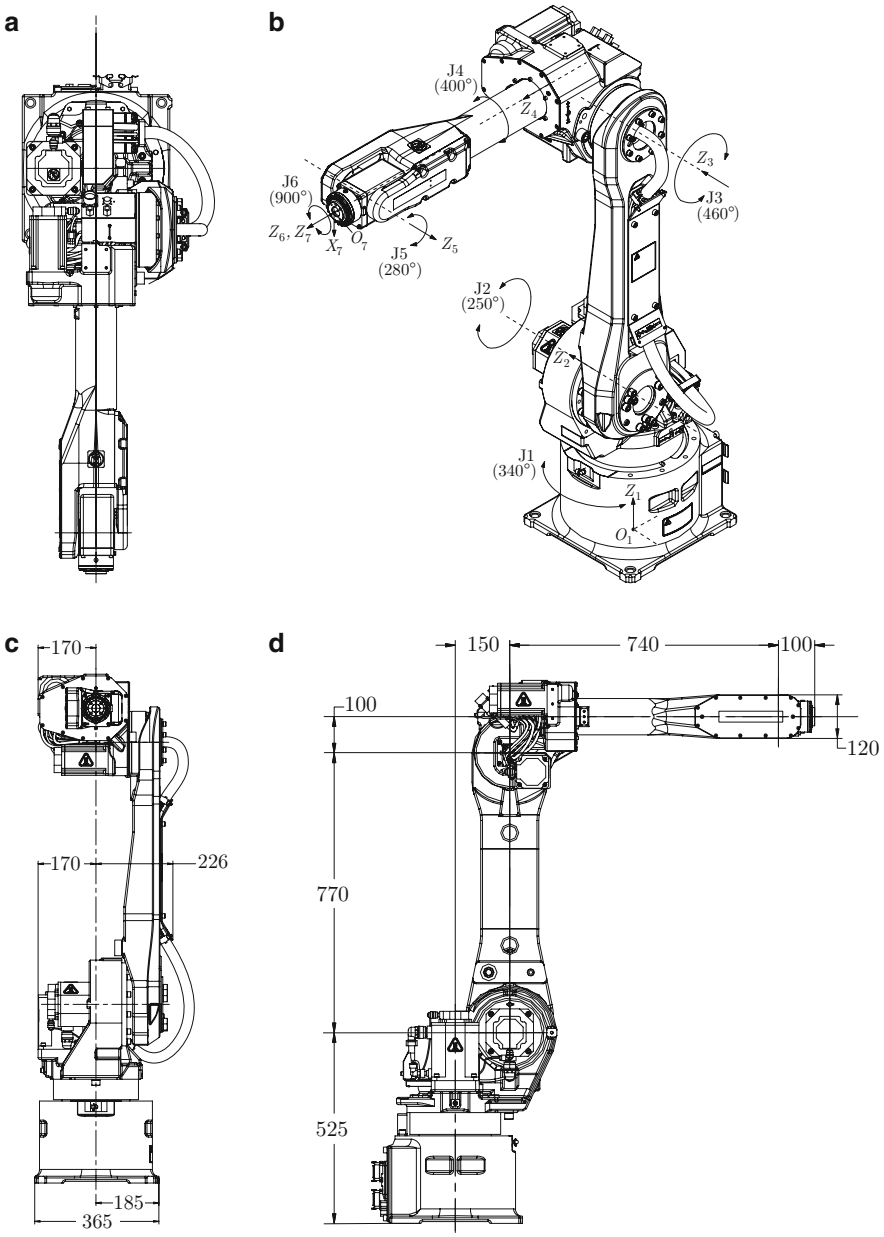

Fig. 4.25 Geometric information taken from the data sheet of an industrial robot: (**a**) the top view; (**b**) an isometric view; (**c**) front view; and (**d**) side view

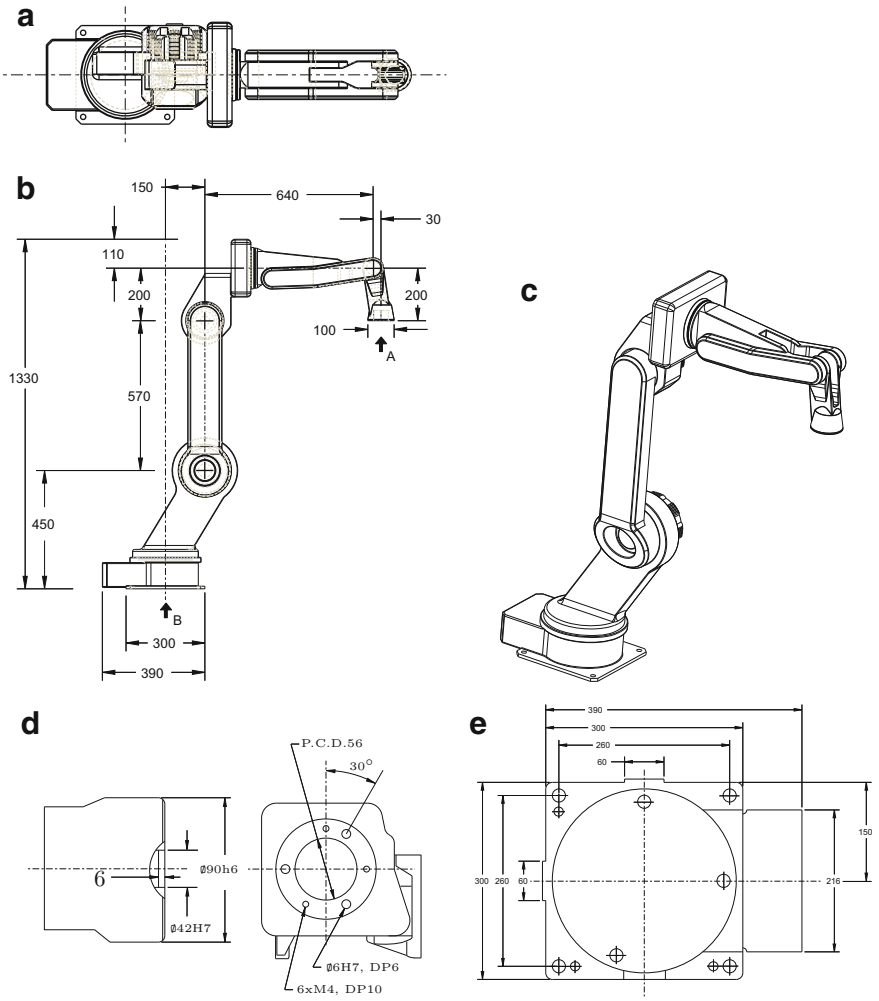

Fig. 4.26 Motoman-EA1400N welding robot: (**a**) top view; (**b**) orthographic projection; (**c**) side view; (**d**) view A, as per sideview; (**e**) view B, as per side view. All dimensions in mm

4.7 An orthogonal spherical wrist has the architecture shown in Fig. 4.20, with the DH parameters

$$\alpha_4 = 90^\circ,\ \alpha_5 = 90^\circ$$

A frame $\mathcal{F}_7$ is attached to its EE so that Z_7 coincides with Z_6. Find the (Cartesian) orientation that can be attained with two inverse displacement solutions $\boldsymbol{\theta}_I$ and $\boldsymbol{\theta}_{II}$, defining the two distinct postures, that lie *the farthest* apart. Note that a *distance* between two manipulator postures can be defined

as the radical of the quadratic equation yielding the two inverse kinematic solutions of the wrist, whenever the radical is positive. Those postures giving the same EE orientation and lying farthest from each other are thus at the other end of the spectrum from singularities, where the two postures merge into a single one. Hence, the postures lying farthest from each other are singularity-robust.

4.8 Given an arbitrary three-revolute manipulator, as shown in Fig. 4.11, its singular postures are characterized by the existence of a line passing through its operation point about which the moments of its three axes vanish—see Exercise 3.3. Note that this condition can be readily applied to manipulators with a simple architecture, whereby two successive axes intersect at right angles and two others are parallel. However, more complex architectures, like that of the manipulator of Fig. 4.15, are more elusive in this regard. Find the line passing through the operation point and intersecting the three axes of the manipulator of Fig. 4.15 at a singularity. *Hint: A singular posture of this manipulator was found in Example 4.4.2.*

4.9 For the *Fanuc Arc Mate 120iB* robot displayed in Fig. 4.25, with the dimensions in mm included therein,

(a) Find its Denavit–Hartenberg parameters, using the Z_i axes suggested in Fig. 4.25b.

(b) Apparently, the robot under study is of the decoupled type. Find all its inverse-displacement solutions for an arbitrary pose of its end-effector, assuming that the operation point is located at a point of $\mathcal{F}_7$ coordinates $[\,0.0,\ 100.0,\ 100.0\,]^T$ mm.

4.10 Shown in Fig. 4.26 is the data sheet of the Motoman-EA1400N welding robot. Under the assumption that the operation point of the robot is located along the axis of the 6th joint, on the flange indicated in **View A**, produce a table with the Denavit–Hartenberg parameters of the robot. N.B.: all lengths are indicated in mm. It is strongly recommended to sketch the robot at an *arbitrary posture* in order to ease the definition of the DH coordinate frames. Is this robot decoupled?